ARTICLES

Spin-transfer measurements of the $\pi\vec{d}\rightarrow\vec{p}p$ reaction at energies spanning the Δ resonance

A. Feltham
Department of Physics, University of British Columbia, Vancouver, British Columbia, Canada V6T 1Z1
and Department für Physik und Astronomie, Universität Basel, 4056 Basel, Switzerland

G. Jones, R. Olszewski,* M. Pavan,† M. Sevior,‡ R. P. Trelle,§ and P. Weber‖
Department of Physics, University of British Columbia, Vancouver, British Columbia, Canada V6T 1Z1

G. J. Lolos, E. L. Mathie, and Z. Papandreou
Department of Physics, University of Regina, Regina, Saskatchewan, Canada S4S 0A2

R. Rui
Dipartimento di Fisica, Università di Trieste, 34127 Trieste, Italy

D. Gill, D. Healey, D. Ottewell, G. Sheffer, G. R. Smith, V. Sossi, G. Wait, and P. Walden
TRIUMF, 4004 Wesbrook Mall, Vancouver, British Columbia, Canada V6T 2A3
(Received 22 July 1996)

The first spin-transfer experiment performed for the $\pi\vec{d}\rightarrow\vec{p}p$ reaction is described. Three spin-transfer parameters for this π-absorption process were determined, K^a_{LS}, K^a_{SS}, and K^a_{NN}, which correspond to the π-production parameters, K^p_{SL}, K^p_{SS}, and K^p_{NN}, of the time-reversed $\vec{p}p\rightarrow\vec{d}\pi$ process. Each observable was measured at a single angle for a number of energies spanning the Δ resonance of this system. The results are compared with the predictions of published partial wave amplitude fits which are primarily based on existing data for the time-reversed $pp\rightarrow d\pi$ reaction, and also with the predictions of two current theories. The failure of these theories to describe the fundamental features of the data clearly demonstrates the need for further theoretical work in this area. [S0556-2813(97)05401-0]

PACS number(s): 24.70.+s, 13.75.Cs, 25.10.+s, 25.40.Qa

I. INTRODUCTION

The study of few-body systems in nuclear physics has provided most of the knowledge concerning the basic interactions between the particles which constitute nuclei. An important example of a few-body reaction is the $NN\rightleftharpoons NN\pi$ process [1], the simplest nuclear reaction involving production or absorption of a real pion. Interest in such processes stems from the fundamental role played by the pion in nuclear interactions [2]. Understanding the absorption/production mechanism for real pions is a necessary prerequisite to understanding the analogous process for virtual pions inside the nucleus. Further, this mechanism provides a means to study the role of excited nucleons inside the nucleus since the absorption/production of a pion is frequently coupled to a Δ, N^*, etc. channel in the intermediate state. In this paper we consider the $pp\rightleftharpoons d\pi$ channel, a process whose intermediate state is dominated by the $N\Delta$ system.

Of the accessible pion production/absorption channels, the $pp\rightleftharpoons d\pi$ reaction is the simplest to study from both the experimental and theoretical points of view. Experimentally, the fact that only two particles, each charged, are involved in the initial and final states, provides not only uncomplicated particle detection but also useful two-body kinematical correlations. Theoretically, the well understood structure of the deuteron enables a thorough treatment of both the initial and final two-particle states.

Several theoretical approaches to calculating the $pp\rightleftharpoons d\pi$ reaction have been attempted. Although some calculations are successful in describing certain features of the data, none are able to fully describe all of the available data [1]. The failure of the various theoretical approaches is most clearly seen in their poor description of the spin-dependent observables [1]. Despite the current difficulties, further improvements to the theoretical understanding of this fundamental reaction will clearly benefit from the extensive data base which currently exists since it can be used to identify

*Present address: Eberline Instruments GmbH, Postfach 1628, 91006 Erlangen, Germany.
†Present address: Laboratory for Nuclear Science, M.I.T., Cambridge, MA 02147.
‡Present address: School of Physics, Univ. of Melbourne, Parkville, Victoria 3052, Australia.
§Present address: Chemische Werke Bayer, Leverkusen, Germany.
‖Present address: IPP/ETH Zürich, PSI, 5232 Villigen, Switzerland.

those processes which theory fails to adequately describe.

In order to extract physical insight from the available data two approaches have been commonly used to characterize the observables in the context of physically relevant parameters. An expansion of the $pp \rightleftharpoons d\pi$ observables in terms of helicity amplitudes has the advantage of requiring only six complex amplitudes, all of which depend on angle as well as energy [3]. An alternative approach involves a partial wave expansion which capitalizes on the coupling of the spin and angular momentum structure of the process and is thus particularly useful for identifying contributing reaction channels [4]. Although this approach involves an ''infinite'' number of partial wave amplitudes (PWA), only those corresponding to small angular momenta contribute significantly near threshold. As these amplitudes depend only on energy, and not angle, they are therefore particulary useful for comparing data characterizing different angular regions.

Prior to our experiment, several partial-wave fits to existing $pp \rightleftharpoons d\pi$ data had been performed [5–7]. Despite the considerable variety of data available at that time, significant uncertainties in the magnitudes and phases of some of the smaller amplitudes persisted. In fact, in order to obtain an unambiguous set of PWA's, some authors resorted to imposing theoretical constraints on the fitting procedure [5] leading to an undesirable theoretical bias in the extraction of their amplitudes.

In order to resolve these difficulties in the fitting procedure, it was clear that additional observables were required, particularly those with enhanced sensitivity to the smaller amplitudes. Emphasis was given to those observables dependent on the spin of the deuteron, of which few existed. In this regard, Blankleider and Afnan [4] showed that spin-transfer observables are particularly sensitive to the smaller amplitudes, as they depend only on bilinear products of large and small amplitudes and are not dominated (as are some other observables) by terms containing the modulus squared of large amplitudes. It was also demonstrated empirically by Bugg [8] that spin-transfer data would be essential for an improved determination of some of these amplitudes. At that time however, no values for such observables existed in the data base, due primarily to the technical difficulties associated with such experiments. Only subsequently did technological developments make such measurements feasible.

Prior to the work described in this paper, four spin-transfer experiments had been carried out, all involving the $\vec{p}p \rightarrow \vec{d}\pi$ reaction. Three were performed at energies below the Δ resonance [9–11] at $T_p =$ 450–580 MeV and the fourth at a single energy, 800 MeV [12], above the resonance. Although these experiments yielded high statistical precision with low background contamination (primarily due to the quality of the proton beams and targets employed), they suffered from complications associated with the measurement of the final state deuteron polarization. In particular, those experiments involving polarimeters which relied on deuteron-carbon scattering [9–11] are subject to the possibility of large systematic errors due to the small values of the deuteron-carbon analyzing power involved. In fact, deuteron-carbon scattering is only marginally sensitive to the vector polarization of the deuteron and is virtually insensitive to the tensor components of the deuteron in the energy range associated with those experiments [13]. In addition, analysis of the results was complicated by the mixing of the deuteron spin components arising from the large relativistic boosts associated with the center-of-mass to lab transformations involved.

In order to provide a new approach to the measurement of these sensitive observables, we considered the possibility of measuring spin-transfer observables of the $\pi d \rightarrow pp$ reaction, a reaction linked to the $pp \rightarrow d\pi$ through the invariance of strong interactions under time-reversal (an invariance which is expected to hold to high precision [14], and one which has been verified experimentally to the level of a few percent in similar few-body systems [15]). A spin-transfer measurement in the $\pi\vec{d} \rightarrow \vec{p}p$ direction has the following advantages.

(1) A proven technique of proton polarimetry [16–18] is available based on the large, well-known analyzing powers of inclusive proton-carbon scattering.

(2) Polarized deuteron targets are readily available. With such targets, significant vector polarizations ($|P| \sim 0.35$) with small but calculable [19] tensor polarization ($|P_T| \sim 0.1$) can be readily obtained.

(3) The polarimeter system is ''self-calibrating'' when analyzing the $\pi d \rightarrow \vec{p}p$ reaction, using an unpolarized target. For this case the protons have a polarization normal to the reaction plane with a value $P_{\mathcal{N}}$ equal to the well-known analyzing powers A_{N0} of the time-reversed reaction.

(4) For this reaction, the fact that the center-of-mass system is almost at rest in the lab is very useful, since the small relative velocity in the lab of the center-of-mass minimizes the effect of the Lorentz boost on the polarization of the proton. The lack of energy loss to the motion of the center-of-mass also permitted us, at TRIUMF, to obtain data spanning the Δ resonance. Such an energy range would not have been possible at TRIUMF if the $pp \rightarrow d\pi$ reaction had been employed.

In this paper, the first measurement of spin-transfer observables obtained in the pion absorption channel is described. The experiment was also the first to study such observables, using a single apparatus, over the whole energy range spanning the Δ resonance in the $pp \rightleftharpoons d\pi$ system. Since the systematic errors characterizing our experimental technique are very different from those of the other spin-transfer measurements, the new results provide an independent consistency check of the various systematic errors for those data published at common energies.

Spin-transfer measurements in the $\pi\vec{d} \rightarrow \vec{p}p$ direction are not without their own distinctive problems, however. These include difficulties associated with the low fluxes typical of pion beams, background resulting from pions interacting with the additional complex nuclei contained within the polarized deuterated butanol target, and precession of the spin of the proton while traversing the magnetic field in the region of the target.

The significantly lower reaction rates resulting from use of pion beams, coupled with the low efficiency of the proton polarimeter (which involves a ''second nuclear scatter'') indicated that the experimental uncertainties would be limited by the available statistics. Consequently, we chose to perform a single angle, high-statistics measurement, at several energies spanning the Δ resonance, for each spin-transfer observable. The most sensitive angular regions for the mea-

surements were determined by examining the results of a variety of partial-wave fits to the existing data. These studies indicated that it was unnecessary to measure each observable over a wide angular range, because in most cases the shape of the angular dependence would be constrained by the other observables in the data set, once the spin-transfer value at some angle was determined.

The particular observables chosen for our measurements were selected for their experimental viability as well as sensitivity to the ambiguities in the amplitudes. The target was designed so that it could be operated with the polarization axis along any one of three Cartesian axes defined with respect to the incident pion beam. These were along the beam direction, or longitudinal (L), two axes transverse to the beam, up/down in the lab or normal (N), and right/left of the beam, or sideways (S). Since simple proton-carbon polarimeters only measure final state polarization components transverse to the direction of motion of the protons (sideways and normal), our measurements were restricted to the set: $\{K_{LS}, K_{SS}, \text{and } K_{NN}\}$, where the first subscript refers to the target polarization and the second to the proton. Parity conservation forbids a transfer of spin between the in-plane and out-of-plane components [20]. The formal definition of these axes is provided in Appendix B.

In order to enable comparison with the results of other measurements, our results are presented in a frame defined by the Madison convention [21]. In such a frame our spin-transfer results are further categorized in terms of a superscript, either an a or p depending on the time order of the reaction under consideration: pion ''a''bsorption, $\pi d\rightarrow pp$, or ''p''roduction, $pp\rightarrow d\pi$. This convention also requires a reversal of the subscripts used to refer to the polarization components of the target and scattered particles. Thus, for example, $K^a_{LS}(\pi\vec{d}\rightarrow\vec{p}p)$ becomes $K^p_{SL}(p\vec{p}\rightarrow\vec{d}\pi)$.

This paper provides a complete description of the experiment, since subsequent to the earlier publication presenting preliminary results [22], the analysis procedure has been modified somewhat and all available data have now been included. A description of the experimental setup, including the detectors, the polarized target, and data acquisition system is provided in Sec. II. Section III describes the analysis procedures used to extract the spin-transfer parameters from the experimental information, and Sec. IV contains a discussion of the uncertainties. Finally in Sec. V, the results are compared with existing PWA fits as well as with two theoretical predictions.

II. THE EXPERIMENT

The experiment was performed on the M-11 pion beamline at TRIUMF. The beam profile at the target typically had a horizontal width of 1.5 cm and vertical width of 1.0 cm (FWHM) [23]. The beam divergencies were typically $\pm 0.67°$ in the horizontal plane and $\pm 3.2°$ in the vertical. The pion rate was typically a few MHz. The experimental layout is illustrated in Fig. 1.

A. The detectors

A two-arm detection system was used. The requirement of coincidence detection of both of the outgoing protons significantly reduced the number of background events which would otherwise trigger the apparatus. The forward arm (A) served as the polarimeter. The backward arm (B) was placed at the appropriate conjugate angle defined by the two-body $\pi d\rightarrow pp$ kinematics. The acceptance of the apparatus (determined by the size of the third wire chamber of arm A) was approximately 40 msr, corresponding to an angular acceptance of about ± 3 degrees.

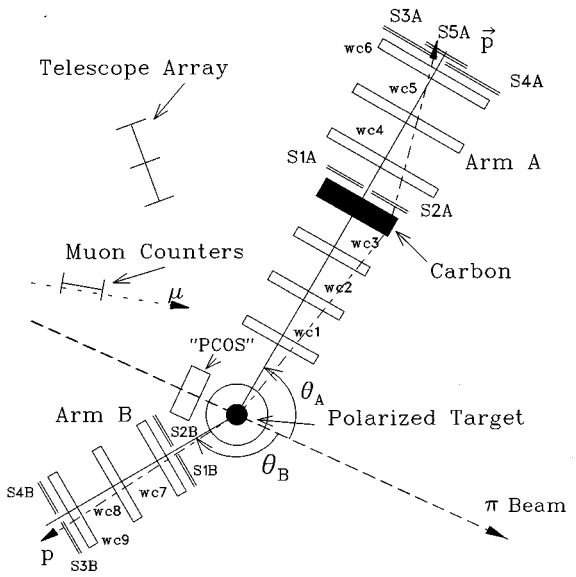

FIG. 1. Layout of experimental area (not to scale). Si(A/B) denote the scintillators and WCi the wire chambers. A typical trajectory for the final state protons is given by the long/short dashed arrows. The relative angles of the detector arms in this figure have been modified for illustrative purposes. The actual values varied depending on the particular energy and configuration [28].

Each arm consisted of a combination of plastic scintillators and wire chambers. The scintillators provided the fast trigger information which was crucial for the event definition and timing, while the wire chambers contributed the position information required for the reconstruction of the proton trajectories.

The wire chambers were *multi-wire delay-line drift chambers* (MWDC's) [24] which offered good spatial resolution over a large area with minimal associated electronics. Each chamber contained two independent wire planes, one to provide the ''x'' and the other the ''y'' position information. Anode and cathode wires were placed alternately along the plane with a separation of 4.06 mm. The anode wires of each plane were connected to the delay line which was maintained at a positive voltage of $\sim$ 2.1 kV. The cathode wires were alternately connected to an ''ODD'' and ''EVEN'' bus and were held at ground potential. The arrival times of the signals propagating to both ends of the anode delay line (t_R, t_L) as well as from the ODD cathode bus ($t_{\rm ODD}$) were recorded. The start for the TDC's was defined by the time of arrival of an event in scintillator S1A or S2A of arm A. From the timing information, the ''hit-wire,'' drift distance (from the hit-wire), and chamber efficiency could be determined [25]. The ''left-right ambiguity'' of the drift distance was resolved using analog signals [25,26] which were also recorded from the cathode busses (ODD, EVEN). Following

TABLE I. Target dimensions (depth×width×height), material surrounding the target (including respective thickness in mg/cm^2), and target angle (with respect to the pion beam) for the various configurations employed.

Config.	Target dimensions (mm^3)	Container material (mg/cm^2)	Shielding wall materials (mg/cm^2)	Targ. rot. angle (deg)
K_{LS}	10×20×20	Teflon (FEP) 66	Cu, mylar, st. steel, Al 155, 18, 201, 452	0
K_{SS}	20×10×20	Teflon (FEP) 66	Cu, mylar, st. steel, Al 214, 18, 201, 452	0
K_{NN}	19×19×14	Mylar 49	Cu, mylar, Kapton, Al 182, 11, 36, 452	12

runs during which the chamber spatial information was calibrated [27–29], position resolutions of better than ± 200 μm were achieved [29].

The wire chambers were grouped into sets of three. Only two wire chambers were required to define a linear trajectory, but the redundancy of an additional chamber increased the overall efficiency of a set since only 2 out of the 3 were required to define a trajectory. The polarimeter arm (A) contained both a set of large (60×60 cm^2) and a set of small (30×30 cm^2) chambers, whereas arm B contained only a set of small chambers. The wire chambers in each set were separated (center-to-center) by 21.0 cm, and the separation between the large and small sets of arm A was 42.0 cm (center-to-center of the nearest chambers). The carbon analyzer, situated at the midpoint between the large and small chambers of arm A, consisted of 30×30 cm^2 graphite sheets ($\rho = 1.71 \pm 0.05$ g/cm^3) of 1 cm thickness. A number of sheets were stacked along the longitudinal axis of the polarimeter producing a total thickness of 5 or 7 cm, depending on the average proton energy for the run in question (the specific choice for analyzer thickness is discussed in Appendix A).

Pairs of scintillators were placed at each end of the set of wire chambers of arm B and at each end of the set of large chambers of arm A (the first pair of scintillators was placed immediately after the carbon analyzer) as shown in Fig. 1. In order to ensure freedom from geometric biases in acceptance, care was taken to ensure that the scintillators were placed symmetrically about the longitudinal axis of the wire chambers. In addition a third scintillator (S5A) was placed behind (and overlapping) the last pair (S3A and S4A on arm A. The common overlap of S5A provided a check of the relative efficiencies of S3A and S4A and gave assurance that the detection probabilities were identical. This was important since a relative difference in the efficiency of S3A and S4A would result in a spatial dependence for the acceptance, and thus a bias in the polarization measurement (see Sec. III A).

Additional detectors were included in the experiment for diagnostic purposes. To independently monitor variations in the pion beam flux ''muon counters'' (two sets) were placed at the exit of the M-11 beam channel to detect the muons coming from those pions decaying in the beam-line, as well as a ''telescope array,'' which pointed at the target, to monitor the scattered particles coming from the target region. To obtain additional information regarding positional shifts and/or broadening of the beam a fast in-beam wire chamber [30,31] was used. The approximate locations of these detectors are illustrated in Fig. 1.

B. The polarized target

The polarized deuteron target [32] used in this experiment had well-understood operational characteristics [19,33,34]. It consisted of a dilution refrigerator, superconducting Helmholtz coils, a microwave source for dynamic nuclear polarization, an NMR circuit for measuring the target polarization, and the target material itself. This material consisted of 95% deuterated butanol (C_4D_9OD) and 5% D_2O, doped with 6×10^{19} atoms/ml of deuterated EHBA-Cr^V complex. It was frozen into beads of 1 mm diameter which were placed in a rectangular plastic container which also supported the copper NMR coil. These beads and their container were immersed in a bath of 94% ^{4}He and 6% ^{3}He, all of which were enclosed in a cylindrical aluminium cup. Surrounding the cup were several thin shielding walls used to provide heat and vacuum barriers. The nature of the material in these walls as well as the dimensions of the target container varied depending on the target configuration employed. The relevant information is summarized in Table I.

The superconducting Helmholtz coils provided a 2.5 T magnetic field which was uniform to 1 part in 10^4 over the immediate target region. The dilution refrigerator maintained the target temperature at a value of ~ 1 K. The temperature was monitored using two separate thermometers, both of which had been calibrated to 1% accuracy prior to the experiment [32].

The deuterons were dynamically polarized using standard microwave techniques [32] with the magnitude of the vector polarization obtained from NMR measurements [32,33]. The target polarization was monitored continually and the average value written to the data tape for each interval of five minutes.

C. The data acquisition

The data acquisition system consisted of standard CAMAC modules in a CAMAC crate together with a CES Starburst ''J-11'' front-end preprocessor which was also connected to a DEC PDP-11/34 computer through the CAMAC bus system. The J-11 executed predefined tasks when it received an EVENT interrupt from the hardware logic. This EVENT interrupt, generated by NIM logic mod-

ules, was produced whenever the scintillator signals satisfied the following logical relationship:

$$\text{EVENT}=(S1B\oplus S2B)\odot(S3B\oplus S4B)\odot[(S1A \oplus S2A)\odot(S3A\oplus S4A\oplus S5A)],$$

where Si(A/B) represents a signal from the appropriate scintillator defined in Fig. 1, $\oplus$ is a logic OR and $\odot$ a logic AND.

One of the functions of the J-11 was to read the ADC, TDC and scaler units contained in the CAMAC crate and to transfer this information to an *event buffer* in its memory. The J-11 also served as a first-level trigger, performing simple calculations on the wire chamber trajectory information in order to reject ''uninteresting'' events before transferring useful data in the event buffer to the PDP-11. The PDP-11 wrote all data accepted by the J-11 to magnetic tape and performed a rudimentary analysis (for on-line diagnostic purposes) of a representative sample of the data.

D. The first-level trigger

The first-level trigger was implemented to reject small-angle scattering events. Multiple Coulomb scattering dominates the small-angle region of the proton-carbon scattering distribution, yet contains essentially no polarization information. Therefore it was advantageous from the point of view of economy and dead-time reduction to reject as many of these events as possible at the front end of the data acquisition system. Such rejection is a common feature of most polarimeter systems of this kind [18,35].

The J-11 preprocessor performed this small-angle rejection by determining the scattering angle of the particle in the carbon analyzer using the hit wire information from the equidistant chambers WC1, WC3, WC4, and WC6 of arm (A). The scattering angle calculation employed a small-angle approximation in order to reduce computation time. The x and y angles were separately calculated:

$$\theta_x\sim\frac{\Delta x}{\Delta z}\quad\theta_y\sim\frac{\Delta y}{\Delta z}.$$

In the case of the K_{LS} and K_{SS} measurements, the events were rejected if *both* θ_x and θ_y were less than 6°. This produced a *square* cut in the (θ_x,θ_y) plane. For the later K_{NN} runs, however, a more efficient *circular* cut was used:

$$\theta^2\sim\theta_x^2+\theta_y^2$$

with events rejected if $\theta^2<(5°)^2$. The effects of such cuts are shown in Fig. 2. A PDP-11 INTERRUPT was generated for those events satisfying the relevant scattering angle requirement. In order to avoid any possible biasing of the accepted events, no additional constraints were imposed on the wire chamber data prior to writing the events to tape. As a result, a significant number of events accepted by the J-11 and subsequently written to tape were identified as ''bad events'' during the off-line analysis and thus rejected.

During each experimental run, a sample of events was collected for which the J-11 preprocessing was disabled. These data are dominated by the small-angle multiple scattering events which possess no azimuthal asymmetry, and thus they were used to check the relative chamber alignment, following techniques described in Sec. III.

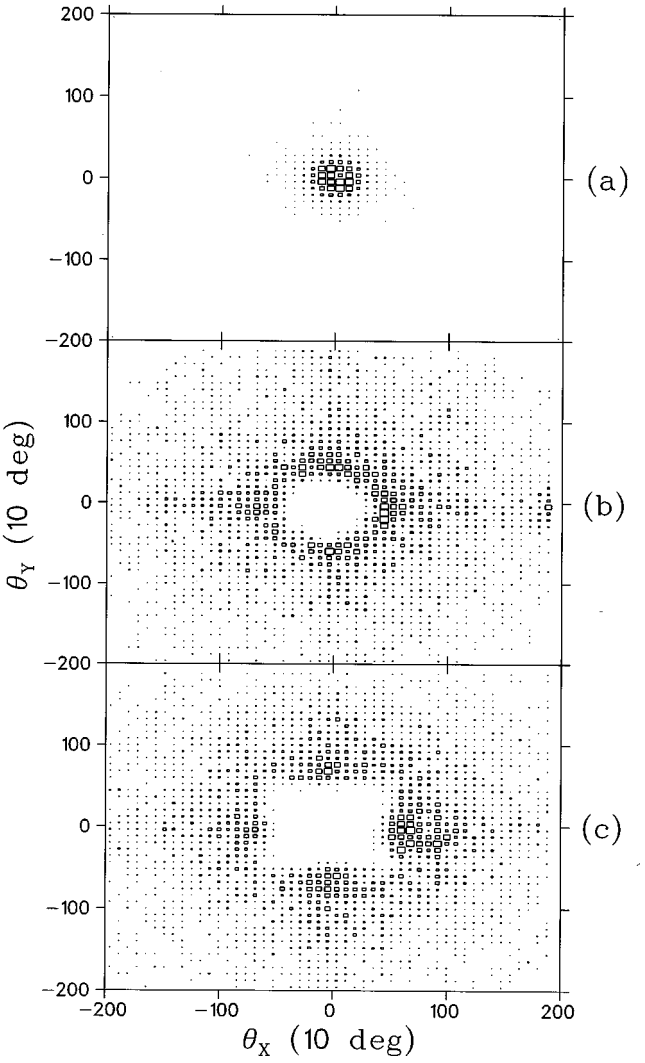

FIG. 2. Scattering angle distributions for data acquired with (a) no J-11 cut, (b) a circular J-11 cut, and (c) a square J-11 cut.

III. DATA ANALYSIS

The extraction of the spin-transfer quantities involved three levels of off-line analysis, with the output of one level used as the input to the next.

The first level of analysis was used to reconstruct the particle trajectories from the data files stored on magnetic tape. Reliable trajectory determination required a careful alignment of the wire chambers. Such an alignment was performed in software using a large sample of proton trajectories. Each straight line trajectory could be defined in terms of two well-known position determinations, the first being the center of the target, which was the mean vertex position of the whole sample of scattered protons (this point was also chosen to be the origin of the analysis coordinate system). The second point was obtained from the spatial coordinates of the trajectory in the fully illuminated WC3, whose absolute position with respect to the pion beam was well known. The absolute positions of WC1 and WC2 were then obtained

TABLE II. Definitions of scattering angles and kinematic variables of the laboratory ''analysis frame'' (see Fig. 3): $\vec{k}_{\pi,i,f,B}$ are the momenta of the incident pion, initial, and final proton trajectories in arm A and the proton of arm B, respectively. $\hat{y}$ is vertically ''up'' in the laboratory (y^I of Fig. 3); $\hat{n}_t$ is the normal to the reaction plane at the deuteron target: $\hat{n}_t=(\hat{k}_\pi\times\hat{k}_i)/|\hat{k}_\pi||\hat{k}_i|$. $\hat{n}_C$ is the normal to the scattering plane at the carbon analyzer: $\hat{n}_C=(\hat{k}_i\times\hat{k}_f)/|\hat{k}_i||\hat{k}_f|$.

Quantity	Definition	Quantity	Definition
θ_{target}	$\cos(\theta_{\text{target}})=\dfrac{\hat{k}_\pi\cdot\hat{k}_i}{\lvert\hat{k}_\pi\rvert\lvert\hat{k}_i\rvert}$	θ_C	$\cos(\theta_C)=\dfrac{\hat{k}_i\cdot\hat{k}_f}{\lvert\hat{k}_i\rvert\lvert\hat{k}_f\rvert}$
ϕ_{target}	$\cos(\phi_{\text{target}})=\hat{n}_t\cdot\hat{y}$	ϕ_C	$\cos(\phi_C)=\hat{n}_C\cdot\hat{n}_t$
sign of ϕ_{target}	$\text{sgn}([\hat{y}\times\hat{n}_t]\cdot\hat{k}_\pi)$	sign of ϕ_C	$\text{sgn}([\hat{n}_t\times\hat{n}_C]\cdot\hat{k}_i)$
$\theta_A+\theta_B$	$\cos(\theta_A+\theta_B)=\dfrac{\hat{k}_i\cdot\hat{k}_B}{\lvert\hat{k}_i\rvert\lvert\hat{k}_B\rvert}$	coplanarity	$\cos(\text{copl.})=\dfrac{\hat{n}_t\cdot\hat{k}_B}{\lvert\hat{k}_B\rvert}$

by interpolating between the two known positions. After aligning WC1,2,3, the crucial alignment of WC4,5,6 was accomplished using those proton events for which the first-level trigger was disconnected. This provided a sample of events which was dominated by protons which had scattered only minimally in the carbon. The average positions of the proton hits in the latter chambers were compared with their expected positions using the projections of the trajectories determined from chambers WC1,2,3. As a check of this procedure, data were obtained during the experiment where the carbon analyzer was removed, allowing for a direct alignment. The two techniques were completely consistent.

After the wire chamber calibration it was then possible to determine reliable trajectories for use in the first part of the main analysis. The trajectories were used to determine the reaction angles and kinematic quantities listed in Table II and illustrated in Fig. 3 as well as the reaction vertices. A reaction vertex was defined to be the point midway between the closest points of approach of two conjugate trajectories.

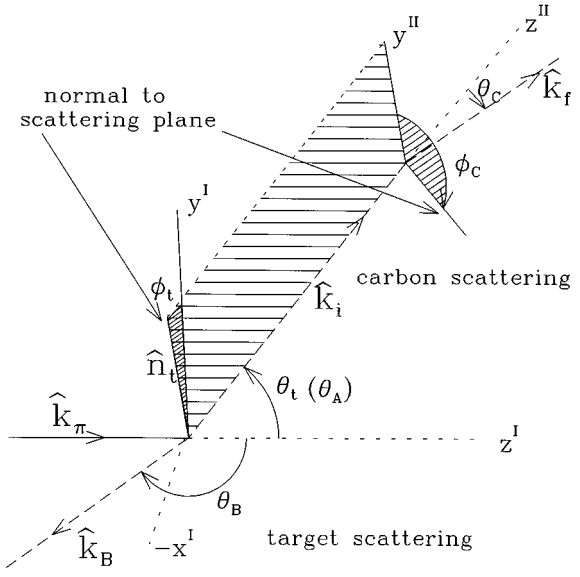

FIG. 3. Definition of coordinate system and angles used in analysis. y^I is vertically ''up'' in the lab, whereas y^{II} of the carbon scattering frame is parallel to $\hat{n}_t$ of the target reaction frame (see Table II). The $\hat{x}$ axis, not shown, is defined from the $\hat{y}$ and $\hat{z}$ axes by the ''right-hand'' rule: $\hat{x}=\hat{y}\times\hat{z}$.

This first part of the analysis also included application of cuts to the data to eliminate those events which failed to meet criteria characteristic of the free $\pi d\rightarrow pp$ reaction, such as the following.

(1) Any ''nonproton'' event, identified by inadequate energy loss in the thin scintillators of arm B (no such cut was employed for the scintillators of arm A, in order to avoid a possible acceptance bias in the polarimeter event sample).

(2) Any event for which insufficient wire chamber information was available. At least 2 of 3 chambers had to ''fire'' for each set (see Table III).

(3) Any event which failed vertex traceback criteria at either the deuteron target or the carbon analyzer. These criteria required each interaction vertex to lie within the resolvable confines of the associated target and also that the minimum distance between the traceback vectors not exceed a characteristic value (typically <1 cm in carbon, and <5 cm at the polarized target). The latter ensured that, within the limitations of resolution, the two trajectories indeed were associated with the same vertex.

(4) Any event which failed the acceptance test in the polarimeter. This test selected only those proton-carbon scattering events for which the azimuthally conjugate ''π-symmetric'' event would have equal probability of detection [i.e., $\text{Acc}(\theta_C,\phi_C)=\text{Acc}(\theta_C,\phi_C+\pi)$], based on the known geometric acceptance of the polarimeter. For each event Acc was assigned either 0 or 1. Without such a restriction, the polarization analysis could introduce false asymmetries due to the finite acceptance of the apparatus [36].

Typically 3–20 % of the original events on tape were remaining in the data sample after the sum of these cuts were applied, depending on the configuration, beam energy, carbon thickness, etc. [28].

A. The polarization analysis

The function of the second analysis level was to extract the scattering asymmetries from the distribution of the polar

TABLE III. Typical wire chamber efficiencies for both individual and sets of chambers.

Chambers	Individual	At least 2 of 3 had fired in set
1,2,3	~ 80%	~ 85%
4,5,6	~ 75%	~ 80%
7,8,9	~ 92%	~ 98%

and azimuthal angles $\{\theta_C,\ \phi_C\}$ of the proton-carbon interaction. The scattering distribution is characterized by the following expression [36]:

$$I(\theta_C,\phi_C,E_p)=I_0(\theta_C,E_p)[(1+\epsilon_S(\theta_C,E_p)\sin\phi_C + \epsilon_N(\theta_C,E_p)\cos\phi_C)]\times \mathrm{Acc}(\theta_C,\phi_C), \quad (1)$$

where $I_0(\theta_C,E_p)$ is the angle and energy dependent unpolarized differential cross section, E_p is the proton kinetic energy at the center of the carbon (determined from the relevant two-body kinematics and the typical energy losses to the center of the analyzer), and $\mathrm{Acc}(\theta_C,\phi_C)$ is the geometric acceptance of the polarimeter after the carbon analyzer. As implied earlier,

$$\mathrm{Acc}(\theta_C,\phi_C)=1$$

for all data surviving the acceptance test of the first level of analysis.

The sideways/normal proton polarizations $(P'_{S/N})$[1] are related to the resulting asymmetry parameters using the known proton-carbon analyzing powers $A(\theta_C,E_p)$ (illustrated in Fig. 4):

$$P'_S=-\epsilon_S(\theta_C,E_p)/A(\theta_C,E_p),$$
$$P'_N=\epsilon_N(\theta_C,E_p)/A(\theta_C,E_p), \quad (2)$$

where the minus sign results from the choice of the coordinate system employed [36]. The efficient estimator method of Besset *et al.* [36] was used for the determination of $\epsilon_S(\theta_C,E_p)$. This approach involves a summation of the data, which are distributed over bins of θ_C, ϕ_C, and E_p, where the contribution of each bin is weighted by its statistical significance. Following Eq. (2), the resulting distribution of $\epsilon(\theta_C,E_p)$ was normalized by the corresponding analyzing power $A(\theta_C,E_p)$ to obtain the polarization value in each $\{\theta_C,\ E_p\}$ bin. The values of $A(\theta_C,E_p)$ used were taken from the parameterization of McNaughton *et al.* [37] (the choice of this particular parameterization is discussed in Appendix A). The polarization values obtained for each $\{\theta_C,E_p\}$ bin were then averaged (proton polarization is independent of these quantities) to provide the *sideways* (P'_S) and *normal* (P'_N) polarizations used later for the spin-transfer determination. The polarizations of the background and foreground components of the data (their identification is discussed in Sec. III B) were carried out separately.

The possible presence of undesirable systematic effects was investigated by evaluating the polarization data (foreground and background separately) as a function of several independent quantities. In particular the possible systematic dependence of the polarization on the following quantities was monitored: carbon polar scattering angle (θ_C), deuteron target scattering angles $(\theta_{\mathrm{target}},\ \phi_{\mathrm{target}})$, and run number.

Typical functional dependencies of polarization with respect to these quantities are shown in Figs. 5(a)–5(d).

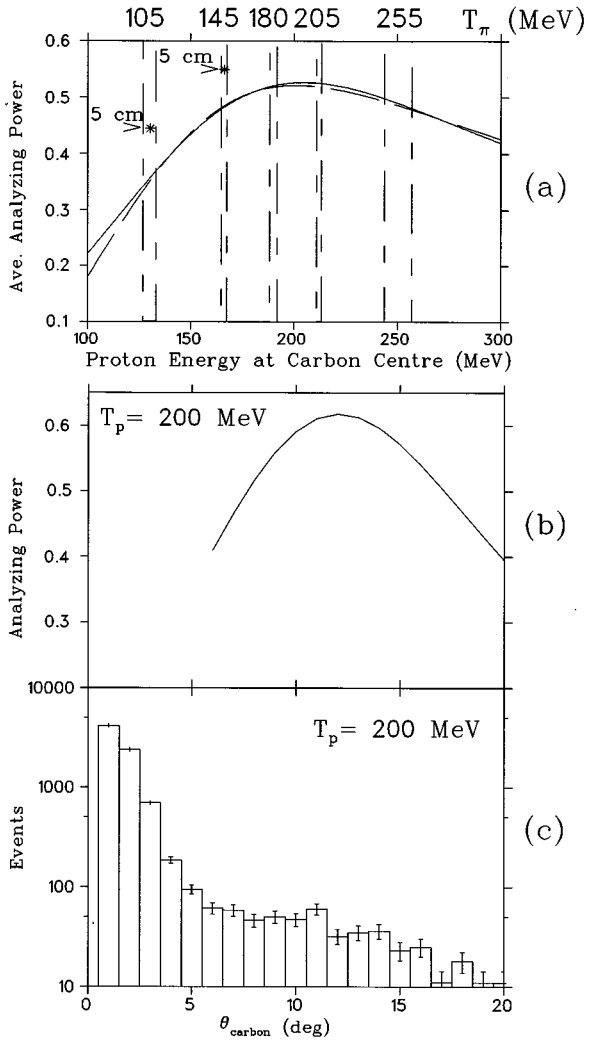

FIG. 4. (a) The energy dependence of proton-carbon analyzing powers (averaged over $5°\leqslant\theta_C\leqslant 19°$). The solid line is due to the parametrization of McNaughton *et al.* [37] (the one used in this analysis), and the dashed line due to Aprile-Giboni *et al.* [43]. Also indicated by the dashed vertical lines are typical proton energy ranges for each pion energy (denoted at top of plot) employed in the K_{NN} configuration. The asterisks (*) indicate the apparent values of the analyzing powers which we have obtained for the analyzing powers of the 5 cm thick analyzer (following the discussion of Appendix A). For proton energies of about 200 MeV are shown (b) the angular dependence of the analyzing power [37], and (c) the angular dependence of the scattering distribution, taken from our data.

B. Background contributions

The second level of analysis also provided the means by which the background contribution could be evaluated. The

[1]Polarizations denoted with a prime (′) refer to the laboratory components as determined by the polarimeter.

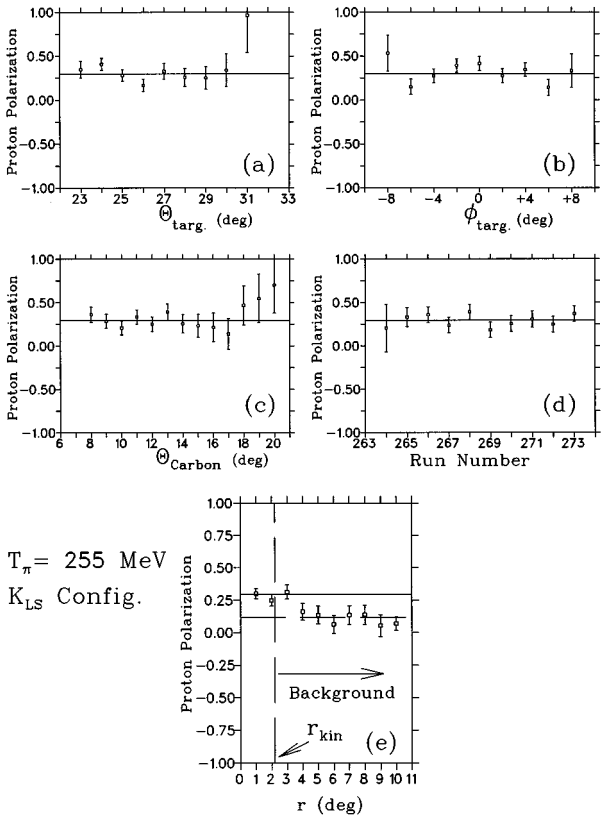

FIG. 5. Examples of checks for systematic dependences in the polarization. The four plots (a)–(d) include only the ''foreground'' data, which correspond to events with $r \leqslant r_{\mathrm{kin}}$ of plot (e). Plot (e) also depicts how the measured polarization changes from the small-angle region of r [see Eq. (3)] which is dominated by foreground events to the large-angle region of r which contains solely background events.

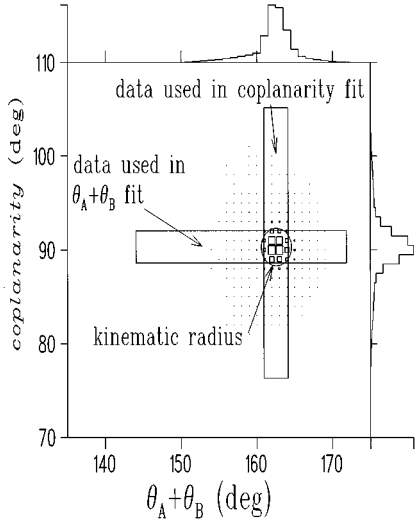

FIG. 6. Slicing technique used in background fits of *coplanarity* and opening angle ($\theta_A+\theta_B$) projections. For example, only the data lying within the vertical box were used in the coplanarity projection of Fig. 2 of Ref. [22].

majority of the background events arose from two-body pion absorption on ''quasideuterons'' within the nuclei (such as carbon or oxygen) present in the target material, reactions which can also produce two protons in the final state (among other possible final states). These protons are energetically similar to those from the free $\pi d \rightarrow pp$ reaction except that their kinematic relationships are greatly broadened due to both Fermi motion of the ''quasideuteron'' and to the fact that momentum is transferred to other particles in the final state.

In the analysis of the free $\pi d \rightarrow pp$ data, two independent kinematic variables were used to help distinguish the background contributions: the opening angle, ($\theta_A+\theta_B$), between the final state protons; and the *coplanarity*, or the extent to which the initial and final state particles trajectories lie within a common reaction plane. Both of these kinematic variables were calculated from the trajectory information (see Table II). In the case of interactions with a free deuteron their values are completely determined by two-body kinematics (within the resolution allowed by the wire chambers, multiple-scattering and magnetic field distortions). The effect of such a two-body final state correlation is illustrated in Fig. 6. It was convenient to define a circle on the plot (the quantities on both axes are expressed in degrees), representing a ''kinematic boundary'' of radius r_{kin}. Acceptable events are those for which $r \leqslant r_{\mathrm{kin}}$, where

$$r = \sqrt{[(\theta_A+\theta_B)-\overline{(\theta_A+\theta_B)}]^2+[\mathrm{coplanarity}-\overline{\mathrm{coplanarity}}]^2} \tag{3}$$

and $\overline{\theta_A+\theta_B}$ and $\overline{\mathrm{coplanarity}}$ are the positions of the peaks of these respective distributions. For each event, Eq. (3) determined the angular deviation from the two-body kinematic peak. By selecting those events with less than a particular value of r_{kin}, foreground events could be effectively distinguished from background events. Since some background events remained under the foreground peak, however, it was necessary to determine their relative numbers and characteristic polarization value in order to assess their contribution to the *true* foreground polarization.

The distribution of the background under the kinematic peak was largely determined by the acceptance of the experimental apparatus, as demonstrated by data from a nondeuterated butanol target.[2] The background distribution from this target was found to be well described by a Gaussian shape. As a result, the shape of the background under the foreground peak (and hence the relative number of background events) could be obtained with confidence by fitting all

[2]The molecular structure of this target was identical to that of the regular target except that ^{2}H was replaced by ^{1}H.

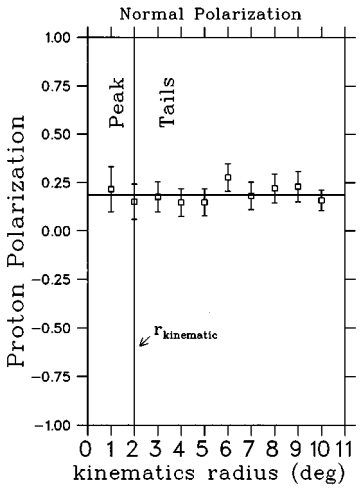

FIG. 7. Kinematical dependence of proton polarization for background events obtained using a nondeuterated butanol target. The values at small kinematic radii are completely consistent with those measured at large radii.

events in the tails ($r>r_{\rm kin}$) of the kinematic distribution to a Gaussian shape, as was demonstrated in Fig. 2 of Ref. [22].

Two separate one-dimensional fits were performed to the slices of data lying within the two elongated boxes shown in Fig. 6. For each fit, the relative amount of background to foreground within the kinematic radius was always consistent and small, typically less than 10%.

The measured polarization P_o is given in terms of the polarization of the foreground events P_f and of the background events P_b by

$$P_o = FP_f + BP_b\,, \tag{4}$$

where F and B are the fractions of events within $r_{\rm kin}$ consisting of foreground and background, respectively. Following the determination of P_b, from those events lying in the tails of the kinematic distribution, P_f could be simply extracted from the data. Analysis of data from nondeuterated background runs demonstrated that the value of the polarization of the background events did not depend significantly on $r_{\rm kin}$, as illustrated in Fig. 7. The results obtained from this analysis are also consistent with those of recent polarization measurements arising from pion absorption on the quasideuteron within ^{3}He [38] and ^{4}He [39]. In the analysis of P_f in Eq. (4), the uncertainty of the correction term BP_b was dominated by the error of B which followed from the conservatively assigned 5% uncertainty applied to the determination of F.

C. Model dependent quantities

The third level of analysis involved extraction of the spin-transfer parameters. In order to relate these parameters to the polarization components measured at the polarimeter, it was necessary to consider a number of kinematic effects.

Although the trajectories of the incident pion beam and outgoing proton beams were well determined experimentally outside the region of the target (resulting in the quantities defined in Table II and Fig. 3), the presence of the magnetic field associated with the polarized target altered the trajectories in the neighbourhood of the target itself. As a result, quantities such as the reaction angle and scattering plane had to be inferred from the trajectory information distant from the target.

In addition, the direction of the proton polarization during its passage to the polarimeter changed as a result of two effects. First, in the rest frame of the proton, the magnetic field of the target induced a Larmor precession of the proton spin vector about an axis defined by the field direction. Second, because of the motion of the rest frame of the proton through the lab (the frame in which the particle is observed), the observed spin direction differed from that in the rest frame by the ''Wigner rotation'' [4]. Both effects were treated in terms of appropriate rotations of the polarization direction as is described in Appendix B.

D. Extraction of spin-transfer observables

As shown in Appendix B, the desired spin-transfer observables are related to the experimentally determined quantities by the following expressions:

$$K_{LS} = \frac{2}{3}\frac{1}{\mathbf{p_d}}\frac{(D^+P_S'^+ - D^-P_S'^-) - (D^+P_N'^+ - D^-P_N'^-)(f_S/f_N)}{g_S - g_N(f_S/f_N)}\frac{1}{(R+1)}, \tag{5}$$

$$K_{SS} = \frac{2}{3}\frac{1}{\mathbf{p_d}\langle\sin\gamma\rangle}\frac{(D^+P_S'^+ - D^-P_S'^-) - (D^+P_N'^+ - D^-P_N'^-)(f_S/f_N)}{g_S - g_N(f_S/f_N)}\frac{1}{(R+1)}, \tag{6}$$

$$K_{NN} = \frac{2}{3}\frac{1}{\mathbf{p_d}\langle\cos\gamma\rangle}\frac{(D^+P_N'^+ - D^-P_N'^-) - (D^+P_S'^+ - D^-P_S'^-)(g_N/g_S)}{f_N - f_S(g_N/g_S)}\frac{1}{(R+1)}, \tag{7}$$

where $P_{S/N}'^{\pm}$ are the polarization components (sideways/normal) measured at the polarimeter and $D^{\pm}$ [from Eq. (B5)] represents the spin-dependent part of the differential cross section. The $\pm$ superscripts describe the direction of the deuteron polarization with respect to the direction of the magnetic field at the target, with $+$ being parallel to the field (i.e., a ''positive'' deuteron polarization). $\mathbf{p_d}$ is the magnitude of the negative deuteron polarization and $R=|\mathbf{p_d^+}|/|\mathbf{p_d^-}|$. The quantities $f_{S,N}$ and $g_{S,N}$ [defined by Eq. (B6)] for the proton and γ for the deuteron relate the respective polarizations in the center-of-mass ''analysis frame'' to the values measured in the laboratory frame (as discussed in Appendix B). In a similar manner, the polarization observable $P_{\mathcal{N}}$ can be extracted:

TABLE IV. Spin-transfer results for $\pi\vec{d}\rightarrow\vec{p}p$ in accordance to the Madison frame. The errors given include statistical errors characterizing the measurement of the proton polarization in the polarimeter together with the statistical and systematic errors associated with the measurement of the deuteron polarization. The results denoted by † were obtained using a 5 cm thick analyzer. They have been extracted using the renormalized proton polarizations as discussed in Appendix A.

T_π (MeV)	θ_{analysis} (deg)	K^a_{LS}	θ_{analysis} (deg)	K^a_{SS}	θ_{analysis} (deg)	K^a_{NN}
105	33±3	-0.122±0.041	N.A.	N.A.	43±3	0.148±0.059†
145	34±3	-0.147±0.041	74±2	0.218±0.055	39±3	0.087±0.073†
180	34±3	-0.268±0.027	75±3	0.174±0.041	37±3	0.186±0.050
205	34±3	-0.256±0.048	75±3	0.239±0.042	36±3	0.149±0.051
255	35±3	-0.238±0.057	76±3	0.301±0.053	35±3	0.069±0.104

$$P_{\mathcal{N}}=\frac{(D^+P'^+_N+D^-P'^-_N)-(D^+P'^+_S+D^-P'^-_S)(g_N/g_S)-(3/2)(R-1)\mathbf{p}_{\mathbf{d}\perp}K_{NN}[f_N-f_S(g_N/g_S)]-2\mathcal{S}_N+2(g_N/g_S)\mathcal{S}_S}{2[f_N-f_S(g_N/g_S)]}, \quad (8)$$

where $\mathbf{p}_{\mathbf{d}\perp}$ is the component of the deuteron polarization orthogonal to the reaction plane.

Included in the expressions leading up to Eqs. (5)–(8) (Appendix B) were the possibilities of instrumental biases denoted by $\mathcal{S}_{S/N}$, biases which could result in the appearance of a nonzero proton polarization where none was expected. These bias terms occur only in Eq. (8); in Eqs. (5)–(7), such systematic contributions cancel because the calculations involve differences between results with opposite deuteron polarizations. The fact that these systematic error terms do appear in the expression for $P_{\mathcal{N}}$ [Eq. (8)] provides an opportunity to assess the size of such errors, through a comparison of the value of $P_{\mathcal{N}}$ to the well-known analyzing powers A_{N0} [40] of the inverse reaction.

After extraction the observables themselves were subjected to two transformations. The first converted the data from the center-of-mass ''analysis frame'' to the conventional Madison frame [21] using straightforward rotations [28]. The values for the spin-transfer parameters [obtained from Eqs. (5)–(7)], expressed in this frame, are listed in Table IV for the various energies and configurations studied in the experiment. The second transformation [20] (based on the coordinate systems shown in Fig. 8) enable the results to be expressed in terms of the time-reversed $pp\rightarrow d\pi$ reaction. The latter transformation was useful for comparing our data with the results of other spin-transfer experiments, as well as for making the comparison between $P_{\mathcal{N}}$ and A_{N0}. The spin-transfer values are presented in this frame later in the report. Table V summarizes the impact of both transformations on the observables.

Table VI summarizes the values of $P_{\mathcal{N}}$ obtained using Eq. (8), together with the corresponding values of A_{N0} from the $\vec{p}p\rightarrow d\pi$ reaction (obtained using an energy and angle dependent parameterization of the existing data [41]). The errors provided for $P_{\mathcal{N}}$ are statistical only as the intention of this table is to indicate the size of possible systematic errors. The errors for the expected value of A_{N0} reflect a 4% uncertainty, typical for many of the measurements of this observable [40]. In general there is very good agreement between the measured normal polarization and the value expected from A_{N0}, and thus there is no evidence of a significant contribution from the systematic error terms [$\mathcal{S}_{S/N}$ in Eq. (8)].

A notable exception, however, is observed for the K_{NN} configuration at the two lowest pion beam energies (T_π=105 and 145 MeV). In this case the values of $P_{\mathcal{N}}$ are found to be significantly higher than the expected values. As is discussed in Appendix A, this discrepancy is attributed to the fact that, unique to these data, a thinner, 5 cm analyzer was employed, and that the published proton-carbon analyzing powers are not adequate for the analysis of these data.

IV. SYSTEMATIC UNCERTAINTIES

Three types of systematic errors were investigated: possible time-dependent shifts in the properties of the apparatus, measurement errors which scale with the magnitude of the proton polarization, and possible polarimeter asymmetry ''bias'' which is independent of the magnitude of proton polarization.

The first item pertains to possible time-dependent changes in the apparatus which include variations in the magnitude of the deuteron polarization to ''drifts'' of the polarimeter electronics. These effects could conceivably lead to the development of an instrumental bias.

Time variations in the polarization of the deuteron target, resulting from changes in the target temperature, the detuning of the polarizing microwave frequency, etc. were handled by monitoring the target polarization continuously with the average value for every five minute interval being stored on magnetic tape. The average polarization for a run set was obtained by weighting each ''five minute'' polarization sample by the number of events accumulated over that period (as recorded by the scalers). The error on the mean was determined appropriately. The magnitude of the variations in the deuteron polarization throughout a run set was typically less than 0.02. Runs in which a rapid depolarization of the target occurred (which happened only rarely) were excluded from further analysis. The final uncertainty quoted for the value of the average deuteron polarization included a

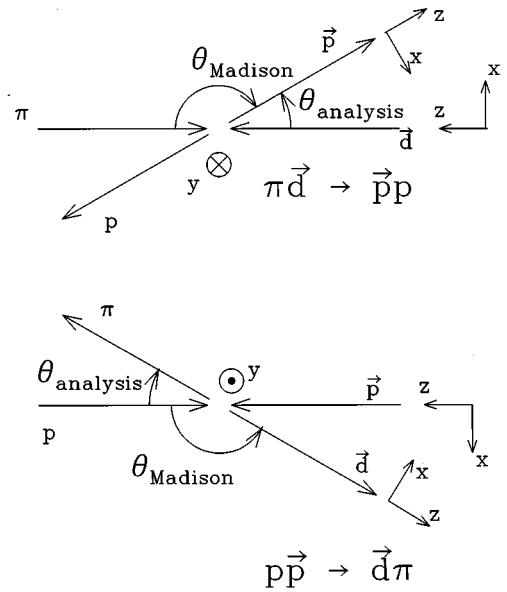

FIG. 8. Comparison of the Madison coordinate systems for the time-reversed reactions: $\pi\vec{d}\rightarrow\vec{p}p$ and $p\vec{p}\rightarrow\vec{d}\pi$. In the Madison convention, the direction of the positive $\hat{z}$ axis is defined by the momenta of those particles whose spins are measured. For each particle whose spin is determined the positive directions of the *x*-*y*-*z* axes in the Madison frame (corresponding to *S*-*N*-*L*) are illustrated.

relative 6% instrumental uncertainty associated with the NMR measurement of the target polarization [42].

To handle the possibility of electronic drifts such as changes in the gains of the signal amplifiers or shifts in the threshold levels of discriminators, etc., the software calibration was performed for each run set (a set consisted of consecutive runs between changes in beam energy or target polarization), or even more frequently if a component of the apparatus was changed. In addition, on-line and off-line diagnostics were employed to indicate the onset of such shifts in the performance of the electronics. In order to identify such time-dependent effects within a run set, the proton polarization was calculated and plotted on a run-by-run basis. Figure 5(d) is a typical time-dependent plot of this kind. No evidence of a significant drift was observed in any of these tests. In addition, selected run sets were repeated several days after their first measurement. All pairs of such ''early/late'' results were found to be in good agreement, again indicating the absence of any significant time-dependent effects.

TABLE V. Transformation of Cartesian spin-transfer observables between the analysis, Madison, and time-reversed Madison coordinate systems. Note that the polarization $P_{\mathcal{N}}$ becomes an analyzing power A_{N0} and that the subscripts of K^a_{LS} and K^p_{SL} are reversed. All quantities are in the center-of-mass frame. The angle, θ, corresponds to θ_{analysis} of Fig. 8.

	$\pi\vec{d}\rightarrow\vec{p}p$			$p\vec{p}\rightarrow\vec{d}\pi$
Analysis frame	$\Leftrightarrow$	Madison frame	$\Leftrightarrow$	Madison frame
$K_{LS}(\theta)$	=	$K^a_{LS}(\pi-\theta)$	=	$-K^p_{SL}(\pi-\theta)$
$K_{SS}(\theta)$	=	$-K^a_{SS}(\pi-\theta)$	=	$-K^p_{SS}(\pi-\theta)$
$K_{NN}(\theta)$	=	$K^a_{NN}(\pi-\theta)$	=	$K^p_{NN}(\pi-\theta)$
$P_{\mathcal{N}}(\theta)$	=	$P_{\mathcal{N}}(\pi-\theta)$	=	$A_{N0}(\theta_\pi)$

TABLE VI. Comparison of measured normal proton polarization $P_{\mathcal{N}}$ at the target with the expected values obtained from a parameterization of A_{N0} data for the $\vec{p}p\rightarrow d\pi$ reaction [41]. The errors associated with A_{N0} represent typical values appropriate to such measurements. Only the statistical errors are listed for $P_{\mathcal{N}}$. The results denoted by † were obtained using a 5 cm thick analyzer. These values were obtained using the published proton-carbon analyzing powers. The scattering angles for which these data were obtained are the same as those listed in Table IV for each configuration and beam energy.

Configuration	Pion energy	Expected value A_{N0}	Measured value $P_{\mathcal{N}}$
K_{LS}	105	0.225 ± 0.009	0.224 ± 0.021
	145	0.399 ± 0.016	0.437 ± 0.024
	180	0.440 ± 0.018	0.420 ± 0.016
	205	0.388 ± 0.016	0.385 ± 0.021
	255	0.280 ± 0.011	0.314 ± 0.028
K_{SS}	145	0.376 ± 0.015	0.384 ± 0.025
	180	0.416 ± 0.017	0.415 ± 0.020
	205	0.352 ± 0.014	0.352 ± 0.020
	255	0.189 ± 0.008	0.195 ± 0.027
K_{NN}	105	0.237 ± 0.009	$0.294\pm0.026^{\dagger}$
	145	0.426 ± 0.017	$0.498\pm0.029^{\dagger}$
	180	0.455 ± 0.018	0.466 ± 0.026
	205	0.394 ± 0.016	0.406 ± 0.023
	255	0.288 ± 0.012	0.298 ± 0.046

The second class of systematic uncertainties are those which scale with the magnitude of the polarization being measured. Such an error could be associated with an incorrect calibration of the apparatus. An obvious example is that of the measurement of the proton polarization P, in the polarimeter, which is inferred from the scattering asymmetry ϵ in terms of the analyzing power A ($P=\epsilon/A$). In this case the inferred polarization is proportional to the measured asymmetry, with a proportionality constant $(1/A)$ which itself is subject to uncertainty. Two sources of error for the analyzing power were considered. One was the uncertainty in the determination of the proton energy at the center of the carbon, resulting in an error in the analyzing power due to the energy dependence of this parameter [significant at lower proton energies, see Fig. 4(a)]. The other also takes into account the possibility that the specific values for the analyzing powers (obtained by other workers [37]) might not be applicable for our polarimeter because, for example, of the dependence of the inclusive proton-carbon analyzing powers on detector parameters such as discriminator thresholds, detector positions, etc.

The proton energies were inferred on the basis of the incident pion energy together with two-body kinematics as discussed earlier. Errors in the proton energy could thus arise from uncertainties in the pion beam position and energy as well as uncertainty in the detector positions. In this regard, the location of both detector arms with respect to the pion beam was known to better than 0.5 degrees and the mean

TABLE VII. Nominal pion beam energy, the true mean beam energy (including energy loss to the center of the target), the corresponding mean proton energy taken from two-body kinematics (including energy loss to the center of the analyzer) together with the expected spread in proton energy distribution. The final column lists the possible error in proton-carbon analyzing powers resulting from uncertainties in the reaction energy.

Configuration	Nominal beam energy (MeV)	True pion Energy at target (MeV) and energy spread ($\pm$ MeV)	Proton energy at carbon (MeV) and energy spread ($\pm$ MeV)	Analyzing power uncertainty (relative) (%)
K_{LS}	105	104.3 ± 4.2	126.3 ± 3.3	4.5
	145	144.2 ± 5.5	162.3 ± 4.3	2.5
	180	179.0 ± 6.5	192.3 ± 5.1	0.8
	205	203.7 ± 7.2	213.6 ± 5.7	0.3
	255	250.3 ± 8.6	253.0 ± 6.9	1.9
K_{SS}	145	143.3 ± 5.5	122.1 ± 3.2	4.6
	180	178.2 ± 6.5	145.4 ± 3.8	3.5
	205	202.9 ± 7.2	161.4 ± 4.1	2.5
	255	249.6 ± 8.6	190.4 ± 4.8	0.7
K_{NN}	105	103.7 ± 4.2	129.8 ± 3.3	4.0
	145	143.7 ± 1.6	166.3 ± 1.3	0.7
	180	178.7 ± 2.0	190.0 ± 1.6	0.3
	205	203.3 ± 1.4	212.0 ± 1.1	0.1
	255	246.7 ± 8.6	250.5 ± 6.7	1.8

value of the pion beam energy was very stable and known to better than 1% [23]. The pion beam was also characterized, however, by a momentum and angular spread [i.e., $\Delta p/p\sim5\%$ (FWTM),[3] $\Delta\theta_x\sim\pm0.67°$, $\Delta\theta_y\sim\pm3.2°$] leading to a concomitant spread in the energy of the outgoing protons. Although the expected values of the proton energies used in the analysis were based on the central energy of the pion beam, the actual mean value of the proton energy distribution might be expected to be somewhat different due to the strong energy dependence of the $\pi d\rightarrow pp$ cross section. This systematic uncertainty in the average proton energy would therefore affect the determination of the proton-carbon analyzing powers. The impact of such an error on the analyzing powers is related to the range of energies involved [see Fig. 4(a)], with the largest effect occurring at the lowest pion energies and largest polarimeter angle position (that for which K_{SS} was measured). Table VII lists the average proton energies at the center of the carbon analyzer (each value includes the energy losses in the target material and carbon), the approximate proton energy spreads, δE (due to the pion energy spread), and the resultant uncertainties in the analyzing power $(\Delta A/A=[1/\langle A(E)\rangle(\Delta A/\Delta E)\times\delta E)$ of the polarimeter, where $\Delta A/\Delta E$ was taken from the slope of the A versus E curve [such as that in Fig. 4(a)]. The inclusion of this error in the analysis was a conservative attempt to include an uncertainty related to the energy dependence of the proton-carbon analyzing powers. This contribution is likely an overestimate since, to first order, the influence on the average value should be minimal. In any case, it was found that the inclusion of these uncertainties did not contribute significantly to the uncertainty in the final spin-transfer results since the measurements were limited primarily by statistics.

In order to verify that the published values of the proton-carbon analyzing powers used here were appropriate to describe our polarimeter, and that no significant energy-dependent errors remained unidentified, protons of known polarization were produced and detected in the polarimeter. These protons, originating from the $\pi d\rightarrow pp$ reaction where an unpolarized deuteron target was employed, had a polarization *normal* to the reaction plane with a value $P_{\mathcal{N}}$ equal to the analyzing power A_{N0} of the time-reversed $p\vec{p}\rightarrow d\pi$ reaction. The value of A_{N0} is well known over the entire kinematic range relevant to our experiment. In the case of an unpolarized deuteron target $P_{\mathcal{N}}$ was determined using a reduced form of Eq. (B6), where the sideways and longitudinal components at the target (P_S and P_L) are necessarily zero and $P_N=P_{\mathcal{N}}$:

$$P_{\mathcal{N}}=\frac{P'_N-\mathcal{S}_N}{f_N}. \tag{9}$$

Due to the considerable time required for each measurement it was not possible to obtain such unpolarized target data for all energies of each configuration. However, the same observable $P_{\mathcal{N}}$ could also be extracted, using Eq. (8), from the data obtained with the polarized target. This made it possible to check the polarimeter for each specific spin-

[3]For the K_{NN} runs at $T_\pi=$ 145 MeV, 180 MeV, and 205 MeV $\Delta p/p$ was $\sim1.5\%$.

TABLE VIII. The measured normal polarization of the protons produced from an unpolarized deuteron target compared with the expected values from A_{N0}. Also listed with each measurement is the average energy of the protons at the center of the carbon indicating the energy region over which this systematic check was performed. The results denoted by † were obtained using a 5 cm thick analyzer. They were obtained using the published analyzing power parameterizations.

Configuration	Nominal pion beam energy (MeV)	Expected value (from A_{N0})	Measured value ($P_{\mathcal{N}}$)	Average proton energy (MeV)
K_{LS}	205	0.388 ± 0.016	0.428 ± 0.038	213.6
K_{SS}	205	0.352 ± 0.014	0.325 ± 0.076	161.4
K_{NN}	105	0.237 ± 0.009	$0.296\pm0.033^{\dagger}$	130.1
K_{NN}	145	0.426 ± 0.017	$0.485\pm0.037^{\dagger}$	166.2
K_{NN}	255	0.288 ± 0.012	0.245 ± 0.059	250.4

transfer configuration and at each energy without the expense of additional measurements.

The values for $P_{\mathcal{N}}$ obtained from the unpolarized [Eq. (9)] as well as the polarized target (Eq. (8)] are listed in Table VI and Table VIII, respectively. In general, the results obtained for $P_{\mathcal{N}}$ in both tables are in good agreement with the expected results inferred from A_{N0} [41]. These results provide independent confirmation of the validity of the published proton-carbon analyzing powers over the range of proton energies relevant to our experiment.

A consistent exception to the good agreement are the data obtained using the 5 cm thick carbon analyzer. For these data, both for polarized and unpolarized deuteron targets, the values of $P_{\mathcal{N}}$ obtained were significantly higher than expected. As discussed in Appendix A, this discrepancy is attributed to the failure of the published parameterizations to describe the analyzing powers for a 5 cm analyzer in this proton energy range. It thus represents a systematic error of the second type described here. It was possible, however, to correct for this scale error using the knowledge of A_{N0} in a manner which is described in Appendix A.

The lack of statistical precision in our measurements made it impossible to distinguish between the small differences of published proton-carbon analyzing power parameterizations available to our polarimeter. To reflect a possible error which might arise if our choice of parameterization was not the most appropriate one, a suitable systematic error contribution was included in the uncertainty analysis. The size of this contribution was determined by the relative difference between two recent analyzing power calibrations [37,43]. Although this contribution to the overall uncertainty is small, it does tend to be more significant at the lower proton energies, as indicated in Table IX.

The third class of systematic errors are those *independent* of the magnitude of the polarization. For example, such an error would arise if there were a bias in the apparatus which introduced an artificial asymmetry to the measurements. In our case, such a bias would manifest itself as a systematic shift in the scattering asymmetry, ϵ. Three types of artificial asymmetry were considered. The first was a possible misalignment of the wire chambers which would result in an angular bias for the trajectory reconstruction and thus an incorrect calculation of scattering angles and corresponding kinematical characteristics. The second was a possible spatial dependence of the detection efficiency within the MWDC's or scintillators for particles which scatter in the latter half of the polarimeter, a dependence which would, if ignored, lead to the generation of erroneous values of ϵ. The final artificial asymmetry considered was a possible acceptance bias due to the front-end data selection of the J-11 preprocessor.

Wire chamber misalignments were corrected by the soft-

TABLE IX. Summary of systematic errors included in the error analysis. Also listed are the average magnitudes of the vector polarization of the target, and their uncertainty.

Config.	Nominal beam energy (MeV)	Target polarization and sign	Anal. power uncertainty arising from error in proton energy (%)	Anal. power uncertainty due to parameterization (%)
K_{LS}	105	$+0.289\pm0.017$	4.5	5.0
		-0.376 ± 0.022		
	145	$+0.281\pm0.018$	2.5	2.0
		-0.352 ± 0.027		
	180	$+0.293\pm0.018$	0.8	2.0
		-0.401 ± 0.024		
	205	$+0.288\pm0.017$	0.3	2.0
		-0.389 ± 0.044		
	255	$+0.288\pm0.018$	1.9	2.0
		-0.383 ± 0.033		
K_{SS}	145	$+0.329\pm0.028$	4.6	5.0
		-0.378 ± 0.040		
	180	$+0.340\pm0.020$	3.5	2.0
		-0.382 ± 0.033		
	205	$+0.328\pm0.020$	2.5	2.0
		-0.394 ± 0.034		
	255	$+0.337\pm0.023$	0.7	2.0
		-0.394 ± 0.024		
K_{NN}	105	$+0.284\pm0.020$	4.0	5.0
		-0.285 ± 0.019		
	145	$+0.293\pm0.018$	0.7	2.0
		-0.286 ± 0.018		
	180	$+0.313\pm0.025$	0.3	2.0
		-0.364 ± 0.022		
	205	$+0.282\pm0.021$	0.1	2.0
		-0.334 ± 0.020		
	255	$+0.288\pm0.018$	0.9	2.0
		-0.289 ± 0.018		

ware calibration (discussed in Sec. III). As a result the chambers were aligned to the extent permitted by their spatial resolution (typically better than 200 μm). Nonetheless an additional analysis was performed, upon completion of the wire chamber calibration, to check the resulting alignment. This check involved searching for a dependence on the azimuthal scattering angle for those events which had experienced little or no scattering in the carbon analyzer ($\theta_C \leqslant 3°$). For these small-angle events, the proton-carbon analyzing power should be zero since such scattering is dominated by the Coulomb interaction. The possibility of deviations from a flat azimuthal distribution due to instrumental effects was tested by fitting the following function to the small angle scattering data:

$$f(\phi) = A + B\cos\phi + C\sin\phi, \tag{10}$$

with A, B, and C as variable parameters. In this equation [which is basically Eq. (1)] the standard small angle asymmetries (ϵ) are given by $\epsilon_N = B/A$, and $\epsilon_S = C/A$. In this analysis these asymmetries were always consistent with zero, within a typical statistical precision of 0.01–0.02. This reaffirmed that the chambers were indeed well aligned.

The possibility of asymmetries introduced as a result of spatial inefficiencies in the polarimeter is more difficult to identify, so steps had to be taken to reduce the likelihood of their occurrence. The detectors of particular concern were those located *after* the carbon analyzer in the polarimeter. Unfortunately, the large wire chambers following the carbon were the least efficient of all the chambers employed (see Table III). In order to check for the possibility of spatially dependent asymmetries, searches were carried out to test for systematic deviations between the proton polarizations calculated for events lying in different spatial regions of the polarimeter. A systematic effect of this kind in fact was observed [28] when the polarization was calculated as a function of the target scattering angles ($\theta_{\text{target}}, \phi_{\text{target}}$). It was caused by a small gap between the scintillators S1A and S2A which immediately followed the carbon analyzer. As illustrated in Figs. 5(a) and 5(b) this problem was eliminated by including the existence of the gap in the acceptance function [defined in Eq. (1)]. This procedure did result, however, in a small reduction in the available statistics.

The use of a J-11 preprocessor to select only large angle scattering events could also lead to the introduction of false asymmetries in the angular region close to the edge of this cut. Such effects could arise from the coarse position resolution characteristic of the on-line software (which did not use drift time information), as well as from the corresponding uncertainties in the chamber calibration employed by the on-line software used to reconstruct the trajectories. The influence of the J-11 cut on the asymmetries for small scattering angles is illustrated in Fig. 9 where the polarization is plotted as a function of θ_C. This problem was removed by implementing an off-line cut on θ_C (which was greater than the value used for the on-line cut) to remove those events lying near the edge of the J-11 cut (typically $\theta_C < 8°$).

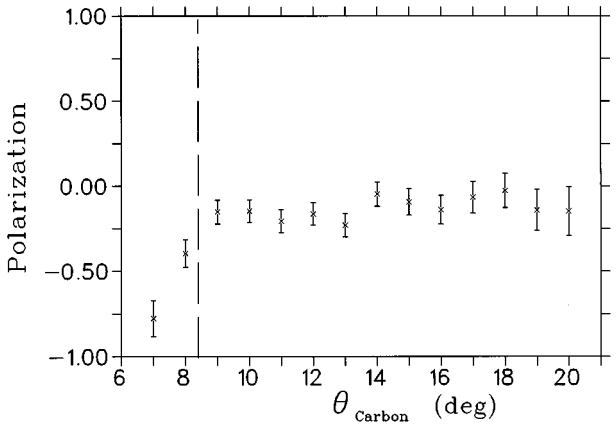

FIG. 9. The dependence of the measured proton polarization on the polar scattering angle in the carbon. As a constant value is expected, the systematic shift seen at smaller angles illustrates the impact of bias introduced by the J-11 preprocessor. The events below 7° degrees were removed by an on-line cut whereas the off-line cut removed those events scattered by angles less than that indicated by the dashed line.

V. DISCUSSION

The contributions of the various systematic errors discussed in the previous section are listed in Table IX. The largest contributions are those associated with uncertainties in the proton-carbon analyzing powers. These arise from the uncertainty in the proton energy at the center of the analyzer combined with the strong energy dependence of the analyzing powers (particularly at low proton energies), together with the question of the applicability to the analysis of our polarimeter data of the particular analyzing power parameterization employed. Since both types of error were always dominated by the statistical errors associated with the measurement of the proton polarization, there was no evidence to suggest a significant systematic bias in the results. In fact, with the exception of those data obtained with a 5 cm thick analyzer (see Appendix A), a quantitative verification of the methods used in this analysis is provided by the agreement between the normal polarization $P_{\mathcal{N}}$ obtained in this experiment and the A_{N0} values characterizing the inverse reaction (Table VI). For the data obtained with the 7 cm thick analyzer, no systematic bias is evident.

Our spin-transfer results, listed in Table X, have been transformed to the inverse $p\vec{p} \to \vec{d}\pi$ reaction following the prescription given in Table V. The errors quoted in Table X include statistical as well as all relevant systematic errors. Our results for K^p_{NN} at $T_p = 783$ MeV can be compared with the measurement of Turpin *et al.* [12] ($T_p \sim 800$ MeV) in Fig. 10. Since K_{NN} is asymmetric about 90° (c.m.) [44], it is clear that the two sets of data are completely consistent. Unfortunately it is impossible to make a direct comparison with other spin-transfer data [9–11], since the other results are complicated by the boost from center-of-mass to the lab and thus contain a mixture of several spin-transfer parameters.

It is possible, however, to compare our results indirectly to the existing data through the predictions of PWA fits which have included the other data in their fit [5,44] (i.e., fits based on data which include the energies: $T_p = 500$, 580, and 800 MeV). As seen in Fig. 11, no significant discrepancy is observed at these energies.

The impact of these new spin-transfer data on the deter-

TABLE X. Spin-transfer results for the $p\vec{p}\rightarrow\vec{d}\pi$ reaction (center-of-mass frame) in accordance with the Madison convention (Table V). The angles listed correspond to center-of-mass angles, whereas the proton energies (lab) are those which are equivalent to the pion energy of column 3 of Table VII for the time-reversed process. The results quoted here include both statistical and all systematic errors (added in quadrature). The results denoted by a † were obtained using a 5 cm thick analyzer. They were extracted using the renormalized proton polarizations as discussed in Appendix A.

T_p (MeV)	$\theta_{\text{deut.}}$ (deg)	K^p_{SL}	T_p (MeV)	$\theta_{\text{deut.}}$ (deg)	K^p_{SS}	T_p (MeV)	$\theta_{\text{deut.}}$ (deg)	K^p_{NN}
500	147±3	0.122±0.042	N.A.	N.A.	N.A.	497	137±3	0.148±0.060†
578	146±3	0.147±0.041	577	106±2	0.218±0.057	577	141±3	0.087±0.073†
648	146±3	0.268±0.028	646	105±3	0.174±0.042	647	143±3	0.186±0.050
697	146±3	0.256±0.048	696	105±3	0.239±0.043	697	144±3	0.149±0.051
791	145±3	0.238±0.057	789	104±3	0.301±0.053	783	145±3	0.069±0.104

mination of the partial wave amplitudes characterizing the $pp\rightarrow d\pi$ reaction can be demonstrated by comparing the results of a PWA fit to a data base which excludes our data, to a fit for which our new data have been included. It is possible in fact to make such a comparison among the PWA's existing in the literature, in that the work of Arndt *et al.* [44] has included our results and the work of Bugg *et al.* [5] did not include our results in their respective data bases (there are also other differences between the two databases employed as new data were released in the meantime). Figure 11 shows, for all three observables, the energy dependence of our data together with the corresponding predictions of these published PWA's. Both PWA predictions are generally in good agreement with each other despite small systematic differences, thus indicating that the existing data now provide adequate constraints for the PWA fits. Moreover, the agreement demonstrates that the theoretical assumptions made by Bugg *et al.* in their work [5] were justified.

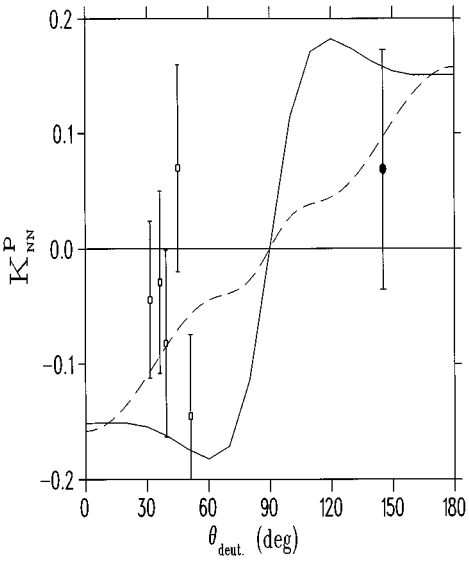

FIG. 10. Comparison of the Turpin data [12] taken at T_p= 800 MeV (□) with the value of K^p_{NN} obtained in this experiment obtained at the equivalent of T_p= 783 MeV (●). The solid line represents the predictions of Arndt *et al.* [44] and the dashed line those of Bugg *et al.* [5] at comparable lab energy (T_p= 800 MeV) and center-of-mass angles.

Although our new data have not had a significant impact on the form of the amplitudes, it is interesting to note that as far as the energy dependence of the spin-transfer quantities is concerned, the fit for which our data were not available (Bugg *et al.* [5]) is systematically somewhat better at describing our data than the fit which includes our data (Arndt *et al.* [44]). This is particularly true for K^p_{NN}, where Arndt *et al.* are systematically higher than Bugg *et al.* and our data, an observation which is supported at 800 MeV by the data of Turpin *et al.* [12] as shown in Fig. 10. This systematic discrepancy suggests an inconsistency between the spin-transfer data and other more precise data which have had a greater influence on the overall shape of the amplitudes (observables measured using the $pp\rightarrow d\pi$ process tend to be of higher precision and are usually obtained for a large number of angular bins).

A noteworthy difference between our data and both PWA predictions is seen in the energy dependence of the observable K^p_{SS} particularly between T_p= 580 MeV and T_p= 700 MeV. In this energy range considerably less spin-dependent

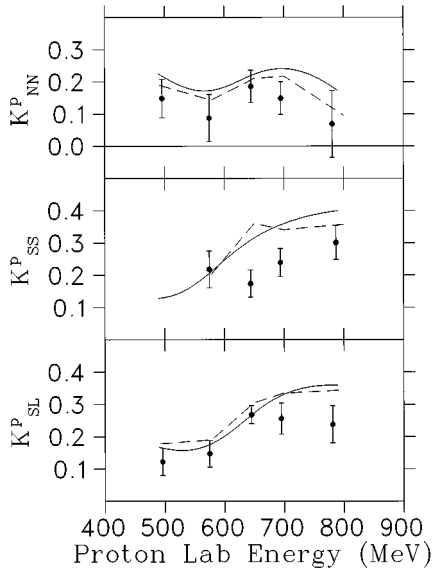

FIG. 11. The spin-transfer observables (expressed in the $p\vec{p}\rightarrow\vec{d}\pi$ Madison frame) as a function of proton lab energy. The curves have the same identity as those in Fig. 10.

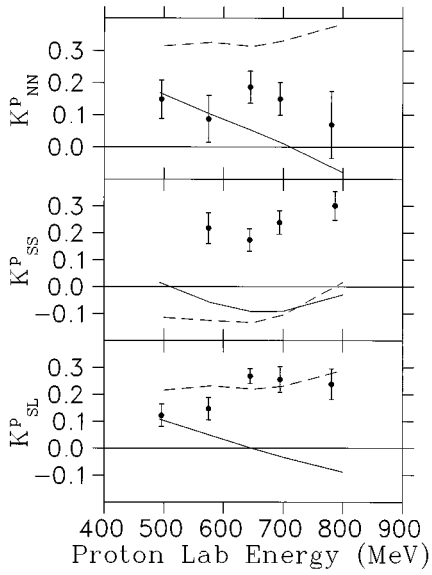

FIG. 12. Our new spin-transfer data are compared with the predictions of two theoretical models. The solid line is that of Blankleider [45] and the dashed line is Niskanen's [46].

data exist, compared to the other energies, and in particular no other spin-transfer data. Since this range spans the peak of the Δ resonance, the observed structure may be signaling some aspect of the behavior of the amplitudes in the region of this resonance which is not predicted by the existing fits.

In Fig. 12, our spin-transfer data are compared with the predictions of two current theoretical calculations [45,46]. Although it is well known that none of the existing calculations adequately describe the spin-dependent observables (A_{N0} is a notable example) it is interesting to compare their predictions to our measurements as well. As seen in Fig. 12, neither of them yield the observed energy dependence of the spin-transfer observables. However, the work of Niskanen [46] does a good job of predicting the observed energy dependence of K^p_{SL} at the angles relevant to our experiment, whereas the calculation of Blankleider does a better job with K^p_{NN}. It is interesting to note that both theories fail in their prediction of K^p_{SS}, even as far as sign is concerned. This difficulty with K^p_{SS}, also noted above with the PWA fits, may indicate a particular sensitivity of this observable to poorly understood details of the reaction.

It is difficult to conclude from such a comparison the exact nature of the theoretical failings, since the observables involved depend so sensitively on the magnitudes and relative phases of a number of amplitudes. It is clear though that our basic theoretical understanding of this fundamental reaction is still too primitive. There have been, however, recent developments that do warrant watching. These include the work of Blankleider and Kvinihidze [47] who are attempting to extend the treatment of the πNN system in a way which is intended to resolve some of the outstanding problems associated with conventional unitary models. In addition, Niskanen has had some success at predicting the related process, $np \to d\pi^\circ$ (near threshold), through the inclusion of heavy meson exchange in his calculation [48]. It would be interesting to see if such contributions also play a role in the region of the Δ for $pp \rightleftharpoons d\pi$. Certainly these as well as future theoretical works will benefit from the reliable PWA's currently available. In this respect, it is increasingly pertinent to compare theoretical predictions with the specific amplitudes rather than the data themselves. Such an approach has already been followed, for example, in the work of Matsuyama and Lee [49].

In summary, this paper demonstrates that spin-transfer measurements performed with the $\pi\vec{d} \to \vec{p}p$ reaction offer a viable approach for studying this fundamental pion absorption/production channel. The advantages of using this reaction over the more conventional pion production channel arise from the availability of good polarized deuteron targets and the well established technique of proton-carbon polarimetry. This technique also provides the capability of verifying the absence of a significant systematic error contribution through the comparison of the measured normal polarization $P_{\mathcal{N}}$ with the well-known analyzing power A_{N0} of the $p\vec{p} \to d\pi$ process. The limitation of the impact of our data on the determination of the PWA's is due primarily to the statistical precision as compared to the other data existing in the database.

In order to overcome the statistical limitations encountered in this work, future experiments employing this technique would benefit from: the increased pion beam intensities now available at some of the meson facilities [50]; recent developments in polarized deuteron target technology [51] which make it possible to routinely achieve deuteron polarizations in excess of 40% using target volumes considerably larger than that which we employed; and the availability of new materials (such as ND_3) which provide an improved ratio of deuterons to other nuclei as compared with the butanol used in this experiment, thus making it possible to reduce the number of background events accepted.

Finally, future experiments of this kind could improve their precision through a better knowledge of the thickness dependence of the proton-carbon analyzing powers. We have obtained evidence that for some of the lower proton energies, higher analyzing powers can be obtained using analyzer thicknesses different from those studied previously [37,43]. Further studies of this kind would be useful for choosing an optimal thickness of analyzer (''Figure of Merit''), thus permitting a more efficient use of the system. Data of this kind are currently available for higher proton energies [13].

ACKNOWLEDGMENTS

We gratefully acknowledge the assistance of Doug Maas and Ivor Yhap for their contributions to the construction and maintenance of the polarimeter, Igor Strakovsky of the Virginia Polytechnic Inst. for interactions regarding the SAID database, and the director of TRIUMF for his support at crucial stages of the project. Financial assistance of the Natural Sciences and Engineering Research Council of Canada is also acknowledged.

APPENDIX A

It is common practice in polarimetry experiments to first calibrate the polarimeter in order to determine the appropriate analyzing powers which characterize the system. In our case, however, it was unnecessary to perform an extensive

calibration of this kind because of the existence in the literature of high-quality parametrizations of analyzing power data obtained for polarimeters very similar to the one we used. Nonetheless our experiment did contain a self-calibrating feature, namely the polarization of the outgoing protons for an unpolarized deuteron target. This is equal to the well-known analyzing power A_{N0} of the time-reversed $\vec{p}p\rightarrow d\pi$ reaction, and thus could be used to verify that the polarimeter behaved as expected. This appendix discusses some important features of the analyzing power parametrizations developed by other workers in this field, in the context of our polarimeter.

We focus on two recently published parametrizations [37,43] appropriate to our system. They differ slightly, but not by an amount which the statistical precision of our measurement could discern. Of these, we chose to employ the parametrization of McNaughton *et al.* [37] because of the similarity between the two polarimeters. In particular, their polarimeter (JANUS) [18] also employed multiwire delay-line drift chambers for trajectory determination and had similar locations for the triggering scintillators. The efficiency of all these detectors is affected by the energy and multiplicity of the final state particles which in turn can influence the acceptance of particular events. This is an important consideration since inclusive proton-carbon scattering produces events characterized by many different kinds of final states, events resulting from both elastic and nonelastic processes. Each process provides a different contribution to the overall average analyzing power.

In the case of the K_{LS} and K_{SS} measurements as well as the three highest energies of the K_{NN} measurement (all of the data which were obtained with a 7 cm thick carbon analyzer), use of the McNaughton parametrization provided excellent agreement between the values of $P_{\mathcal{N}}$, measured for the $\pi d\rightarrow\vec{p}p$ reaction, and those expected from published values of A_{N0} which characterizes the inverse reaction (see Sec. III D). For the two lowest energies ($T_\pi=105$, 145 MeV) used in the K_{NN} measurements, however, a 5 cm thick carbon analyzer was used in order to reduce the energy loss of the protons in the carbon, thereby increasing the effective analyzing powers which are strongly energy dependent at these energies. Interestingly, for the data taken with this 5 cm thick analyzer, both the parametrization of McNaughton *et al.* [37], and that of Aprile-Giboni *et al.* [43], yielded results for $P_{\mathcal{N}}$ which were significantly higher than the corresponding values expected from A_{N0}, as illustrated in Fig. 13. This suggests that the proton-carbon analyzing powers pertaining to the 5 cm thick analyzer, in the proton energy region appropriate to these measurements (see Table VII), are in fact greater than the values indicated by the published parametrizations.

Before we could conclude that the knowledge of the analyzing powers for 5 cm thick analyzers at lower energies is not well established, the possibility of systematic errors affecting our system had to be considered. Use of arguments such as those discussed in Sec. IV enabled us to rule out the presence of time and spatial dependencies in our measurement. Moreover, the possibility of an asymmetry bias could be eliminated for two reasons. On the one hand, the effect of such a bias should be evident in all the data, regardless of the beam energy, since the same apparatus was used throughout

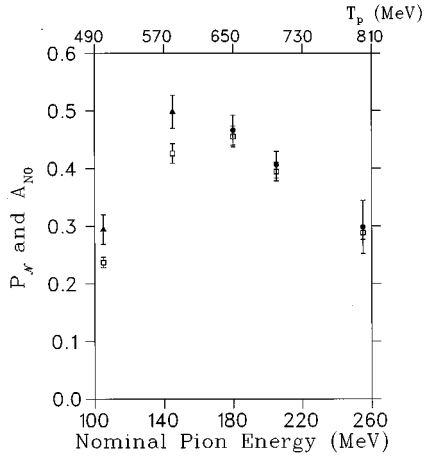

FIG. 13. For data obtained from a polarized deuteron target, the measured polarization $P_{\mathcal{N}}$ (solid points) is compared with the expected value obtained from the analyzing power A_{N0} (open points). The solid $\triangle$ points correspond to data taken with the 5 cm thick analyzer. All values of $P_{\mathcal{N}}$ shown were obtained using the analyzing power parameterization of McNaughton *et al.* [37]. The upper horizontal scale refers to the lab energy of the protons for A_{N0} ($\vec{p}p\rightarrow d\pi$) whereas the lower scale refers to the lab pion beam energy for $P_{\mathcal{N}}$ ($\pi d\rightarrow\vec{p}p$).

the experiment. On the other, such a bias [$\mathcal{S}_{S/N}$ in Eq. (B15)] would be twice as significant for the values of $P_{\mathcal{N}}$ obtained from the analysis of polarized deuteron target data as compared to those obtained from an unpolarized target. In fact no disagreement is observed between the results obtained for the polarized and unpolarized targets (compare Tables VI and VIII).

The observation of this systematic discrepancy associated with the data obtained using the thinner analyzer prompted an examination of the reliability of the analyzing power parametrizations employed in the analysis of data taken with a 5 cm analyzer. Such parametrizations are purported to be independent of the carbon thickness, with the only dependence being on the scattering angle and the proton energy at the center of the carbon [37,43]. Indeed both parametrizations mentioned here resulted from data sets obtained with analyzer thicknesses ranging from 3 to 13 cm. For the case of the 5 cm analyzer, however, there are no published data for proton energies as low as those produced in our 5 cm analyzer measurements. The nearest example was obtained by Aprile-Giboni *et al.* [43] at $T_p=187$ MeV (roughly 20 MeV higher energy than our highest 5 cm data, see Table VII). Although these data do not appear to be significantly higher than their published parametrization, it is interesting that the authors report this particular data set to be in poor statistical agreement, and thus have omitted the set from their fitting work. It should also be noted that their paper [43] comments on the sensitivity of the analyzing powers to the thickness of the analyzer at proton energies below $T_p=170$ MeV. This is in fact the region where our measurements were performed.

The lack of pertinent published data obtained with a 5 cm analyzer, as well as the observation particular to our own 5 cm analyzer data of a systematic deviation of the measured polarization $P_{\mathcal{N}}$ from its expected value, reinforce the conclusion that the published analyzing power parametrizations

TABLE XI. List of renormalization values R_A (obtained from the unpolarized target data) used in the evaluation of the K_{NN} data which were obtained using a 5 cm thick analyzer. Also listed are the reevaluated results for $P_{\mathcal{N}}$ (obtained from the polarized target data, and to be compared with Table VI) and the expected value from A_{N0}.

T_π (MeV)	$\langle T_p \rangle$ (MeV)	R_A	$P_{\mathcal{N}}$	A_{N0}
105	130	0.80 ± 0.10	0.235 ± 0.029	0.237 ± 0.009
145	166	0.88 ± 0.08	0.437 ± 0.037	0.426 ± 0.017

are not reliable for the analysis of our lower-energy ($T_p < 170$ MeV) proton data obtained with a 5 cm analyzer. In our experiment, however, the availability of the $P_{\mathcal{N}}$ data obtained from an unpolarized deuteron target meant that a reliable means to ''recalibrate'' the proton polarization was available. Such data were available for both data sets where the 5 cm analyzer was employed (K_{NN} at $T_\pi = 105$, 145 MeV).

The recalibration was carried out employing the standard relationship between the polarization and the measured scattering asymmetry [Eq. (2)]. First of all it was assumed that the ''true'' analyzing power distribution $A^{\text{true}}(\theta_C, E_p)$ had the same relative energy and angular dependencies as that of the parametrization $A^{\text{param.}}$ (an assumption which is supported by the lack of observation of any such trends in the polarization plots of the kind shown in Fig. 5 for these 5 cm data). In this case the two distributions can be trivially related through a multiplicative factor: $A^{\text{param.}}(\theta_C, E_p) = R_A A^{\text{true}}(\theta_C, E_p)$. The true polarization $P'_{S/N}$(true) can thus be obtained by multiplying the measured polarization $P'_{S/N}$(measured) [from Eq. (2)] by this same factor.

To obtain the factor R_A, the polarization results obtained from the unpolarized deuteron target were exploited [see Eq. (9)]. For these data the true value of the normal polarization P'_N(true) can be equated to A_{N0} of the time-reversed process, since this corresponds to the result one would expect if the correct analyzing power distribution were in fact known. Thus,

$$P'(\text{true}) = A_{N0} = \left(\frac{P'_N(\text{measured}) - \mathcal{S}_N}{f_N} \right) \times R_A , \quad \text{(A1)}$$

where for the K_{NN} configuration, $f_N \sim 1$ and $\mathcal{S}_N \sim 0$ and so, $R_A = A_{N0}/P'_N(\text{measured})$. Since the distribution of events with respect to the proton energies and angles (required for the analyzing powers) is essentially independent of the polarization state of target, it is possible to apply this correction [obtained through Eq. (A1)], at a given pion beam energy, to the data obtained using the polarized target. The scale factor, R_A, would also apply to the correction of the sideways polarization P'_S however for the K_{NN} configuration this component did not contribute significantly.

In Table XI the values obtained for R_A are listed at the two energies for which the 5 cm analyzer was used. As a consistency check for R_A, this correction procedure was applied to the case of the data obtained from the polarized target and a corrected value for $P_{\mathcal{N}}$ was extracted [Eq. (8)]. As can be seen in the last two columns of Table XI, excellent agreement with A_{N0} is now obtained with the polarized target data. This demonstrates consistency between all of our 5 cm analyzer data.

The correction factor R_A was subsequently used to correct the measured proton polarizations, employed in the determination of the K_{NN} values listed in Tables IV and X for pion beam energies of $T_\pi = 105$ and 145 MeV. The use of the corrected proton polarization values in Eq. (7) resulted in a net decrease in the extracted spin-transfer values of 20% and 12%, respectively, for the $T_\pi = 105$ and 145 MeV data sets. This procedure also increased the errors attributed to K_{NN} at these energies due to the experimental uncertainty in the determination of R_A ($\sim 10\%$).

In summary, our observation of a thickness dependence in the proton-carbon analyzing powers for proton energies $T_p < 170$ MeV, confirms the earlier observation of Aprile-Giboni *et al.* [43] concerning the existence of such a dependence in this energy region. Quantitatively we find that the correct values for the analyzing powers appropriate to our 5 cm thick analyzer are 10–20 % larger than those expected from current parametrizations of proton-carbon analyzing powers [see Fig. 4(a) for a comparison]. This is in contrast to the situation for our data taken with the 7 cm thick analyzer, where the existing parametrizations work well. The apparent increase in the 5 cm analyzing powers over the parametrizations (obtained from measurements which employed both thicker and thinner analyzers) could arise as a result of the reduced multiple small-angle scattering (which tends to wash out polarization information) when compared with the thicker carbon data, while retaining the ability to filter out the lower energy inelastic events which contribute a smaller asymmetry [43] (thinner analyzer data would include more of such low asymmetry events). Our data in fact suggest that any future measurements of proton polarization in the energy region: $T_p < 170$ MeV should consider use of 5 cm thick carbon because of the significant improvement in the analyzing power which results. This should be accompanied, however, by a careful calibration of the analyzing powers for the 5 cm thick carbon, as very little relevant information is currently available at these energies in the literature.

APPENDIX B

In this appendix the algebra employed to extract the spin observables from the experimental data is reviewed. For this discussion all quantities listed, unless otherwise indicated, are expressed in a coordinate system referred to as the center-of-mass ''analysis frame'' (COMAF). This frame is the center-of-mass equivalent to the lab ''analysis frame'' described in Fig. 3 except that in this case the momenta are expressed in the center-of-mass (these variables are given the superscript *). The axes of the COMAF are defined in terms of the kinematic variables in the following manner:

$$L \equiv \hat{k}^*_\pi , \quad N \equiv \hat{k}^*_\pi \times \hat{k}^*_p , \quad S \equiv N \times L .$$

The COMAF is essentially that to which the standard Madison convention [21] applies, except for the definition of the longitudinal axis L. In the Madison convention the L axis is defined by the momentum of the polarized particle, in this

case the deuteron (thus for the Madison frame: $L=\hat{k}_d^*=-\hat{k}_\pi^*$). The transformations between these frames of the relavent observables are given in Table V.

In the COMAF the proton polarizations (P_S and P_N) at the target can be related to the vector ($\mathbf{p}_S$, $\mathbf{p}_N$, $\mathbf{p}_L$) and tensor ($\mathbf{p}_{NL}$, $\mathbf{p}_{SN}$, $\mathbf{p}_{SL}$, $\mathbf{p}_{LL}$, $\mathbf{p}_{SS}-\mathbf{p}_{NN}$) polarization components of the deuteron and the physics of the reaction, in terms of the spin-transfer (K), analyzing power (P), and polarization ($P_{\mathcal{N}}$) terms, as well as the polar scattering angle θ [52]:

$$P_S(\theta)=\frac{I_o(\theta)}{I(\theta,\phi)}\left[\frac{3}{2}\mathbf{p}_L K_{LS}(\theta)+\frac{3}{2}\mathbf{p}_S K_{SS}(\theta)+\frac{2}{3}\mathbf{p}_{NL}K_{(NL)S}(\theta)+\frac{2}{3}\mathbf{p}_{SN}K_{(SN)S}(\theta)\right], \tag{B1}$$

$$P_N(\theta)=\frac{I_o(\theta)}{I(\theta)}\left[P_{\mathcal{N}}(\theta)+\frac{3}{2}\mathbf{p}_N K_{NN}(\theta)+\frac{1}{2}\mathbf{p}_{LL}K_{(LL)N}(\theta)+\frac{2}{3}\mathbf{p}_{SL}K_{(SL)N}(\theta)+\frac{1}{6}(\mathbf{p}_{SS}-\mathbf{p}_{NN})[K_{(SS)N}(\theta)-K_{(NN)N}(\theta)]\right], \tag{B2}$$

where $I(\theta)$ is the polarized differential cross section:

$$I(\theta)=I_o(\theta)\left[1+\frac{3}{2}\mathbf{p}_N\overline{P_N(\theta)}+\frac{\mathbf{p}_{LL}}{2}\overline{P_{LL}(\theta)}+\frac{2}{3}\mathbf{p}_{SL}\overline{P_{SL}(\theta)}+\frac{1}{6}(\mathbf{p}_{SS}-\mathbf{p}_{NN})\overline{[P_{SS}(\theta)-P_{NN}(\theta)]}\right] \tag{B3}$$

and $I_o(\theta)$ is the unpolarized cross section. These expressions also contain an azimuthal dependence which has been suppressed in the above, a dependence which varies with the particular orientation of the target polarization and the out-of-plane acceptance of the apparatus. Since the latter is small, this azimuthal dependence is accounted for by appropriate projections of the deuteron polarization components, a procedure which is described in the paragraphs which follow.

The relationship between the Cartesian components of the deuteron polarization and the magnitudes of its vector, $|\mathbf{p}|$, and tensor, $|\mathbf{p_T}|$, values are given in terms of the COMAF kinematic variables by the following [52]:

$$\mathbf{p}_L=|\mathbf{p}|\cos\beta,\quad \mathbf{p}_{NL}=\frac{3}{2}|\mathbf{p_T}|\sin\beta\cos\beta\cos\gamma,$$

$$\mathbf{p}_S=-|\mathbf{p}|\sin\beta\sin\gamma,\quad \mathbf{p}_{SN}=-\frac{3}{2}|\mathbf{p_T}|\sin^2\beta\sin\gamma\cos\gamma,$$

$$\mathbf{p}_N=|\mathbf{p}|\sin\beta\cos\gamma,\quad \mathbf{p}_{SL}=-\frac{3}{2}|\mathbf{p_T}|\sin\beta\cos\beta\sin\gamma,$$

$$\mathbf{p}_{LL}=\frac{1}{2}|\mathbf{p_T}|(3\cos^2\beta-1),\quad (\mathbf{p}_{SS}-\mathbf{p}_{NN})=-\frac{3}{2}|\mathbf{p_T}|\sin^2\beta\cos2\gamma, \tag{B4}$$

where the $|\mathbf{p_T}|$ is related to $|\mathbf{p}|$ by [19]: $|\mathbf{p_T}|=2-\sqrt{4-3|\mathbf{p}|^2}$, so for $|\mathbf{p}|\sim0.35$ a value of $|\mathbf{p_T}|\sim0.1$ is obtained. β is the angle between $\hat{k}_\pi^*$ and the deuteron polarization vector, $\hat{\mathbf{p}}^*$ (in all cases $\hat{\mathbf{p}}^*$ was parallel to the direction of polarization in the lab since both were either parallel or orthogonal to the direction of boost between the frames), and γ is the angle between $\hat{\mathbf{p}}^*\times\hat{k}_\pi^*$ and the ''S'' axis. In this experiment the value of β was constrained to be 0° for longitudinal (L) and 90° for transverse (S,N) target polarizations. The angle γ depended on the direction of the vector polarization as well as the directions of the initial and final state particle momenta, quantities which are affected by the magnetic field of the target and the finite acceptance of the detectors. These effects are treated in detail later in this appendix.

In this experiment, the values of β and the typical range of γ were such that the only non-negligible deuteron tensor component [Eq. (B4)] was $\mathbf{p}_{LL}$, together with an additional contribution from ($\mathbf{p}_{SS}-\mathbf{p}_{NN}$) for the case of the K_{NN} configuration. The other tensor components of Eq. (B4) did not play a role in our measurements.

In Eq. (B3) the terms in square brackets varied only slightly over the limited acceptance of the detector. As a result their contribution was replaced by a weighted average, D, so that

$$\langle I(\theta,\beta,\gamma)\rangle=I_o(\theta)\times D. \tag{B5}$$

The values of the analyzing powers used in Eq. (B3) (for the determination of D) were those predicted from the best PWA description of the reaction available at the time of data analysis [5]. The vector analyzing power ($\overline{P_N}$) was well determined by the PWA's due to the considerable high quality data [53] existing in the data base. For the tensor analyzing powers, however, no measurements exist. A ~2% statistical and ~4% systematic uncertainty has been estimated [5] as applicable to these quantities, since they are highly constrained by existing spin-correlation data. However, in this

analysis, a more conservative 6% overall relative uncertainty was assigned to these quantities.

The proton polarizations measured in the laboratory frame at the polarimeter (see Fig. 3) are related to the corresponding COMAF proton polarizations produced at the target (by the $\pi d \to pp$ reaction) through the following expressions:

$$P'^{+}_{N} = f_N P^{+}_{N} + g_N P^{+}_{S} + h_N P^{+}_{L} + \mathcal{S}_N ,$$

$$P'^{-}_{N} = f_N P^{-}_{N} + g_N P^{-}_{S} + h_N P^{-}_{L} + \mathcal{S}_N ,$$

$$P'^{+}_{S} = f_S P^{+}_{N} + g_S P^{+}_{S} + h_S P^{+}_{L} + \mathcal{S}_S ,$$

$$P'^{-}_{S} = f_S P^{-}_{N} + g_S P^{-}_{S} + h_S P^{-}_{L} + \mathcal{S}_S . \qquad \text{(B6)}$$

Here the superscript $\pm$ denotes the direction of deuteron vector polarization (its natural ''positive'' polarization being denoted as $+$), the primed ($'$) quantities $P'_{N,S}$ are the laboratory polarization components measured at the polarimeter, and the unprimed $P_{N,L,S}$ are the (COMAF) proton polarizations at the target [from Eqs. (B1) and (B2)]. The coefficients f_i, g_i, and h_i represent the couplings (the net effect of all spin rotations, R_j) between the N, S, L center-of-mass components at the target and the ith ($i \in N,S$) polarimeter component in the lab:

$$f_i = \{[\Pi_j R_j]\hat{N}\} \cdot \hat{i},$$

$$g_i = \{[\Pi_j R_j]\hat{S}\} \cdot \hat{i},$$

$$h_i = \{[\Pi_j R_j]\hat{L}\} \cdot \hat{i}.$$

These spin coupling coefficients were determined by integrating, over the proton paths, the BMT equations [54] which describe the incremental change in the spin direction of a proton as a result of its motion in the magnetic field of the target. The coefficients also include the effect of a Wigner rotation [4] of the spin components for the boost (which is small due to the large mass of the deuteron in the initial state) from the COMAF to the lab frame where the BMT equations were utilized. Equation (B6) also include quantities $\mathcal{S}_{S/N}$ which represent possible instrumental asymmetries due to the polarimeter, which could yield systematic biases independent of the sign of the vector polarization.

The dependence, in the COMAF, of the proton polarization on the polarization of the deuteron [as described by Eqs. (B1) and (B2)] was introduced to expressions (B6) after the following convenient simplifications:

$$P^{\pm}_{N} = \frac{P_{\mathcal{N}} \pm \mathbf{p}^{\pm}_{\mathbf{d}\perp} K_N}{D_{\pm}}, \quad P^{\pm}_{S} = \frac{\mathbf{p}^{\pm}_{\mathbf{d}\parallel}}{D_{\pm}} K_S , \quad P^{\pm}_{L} = \frac{\mathbf{p}^{\pm}_{\mathbf{d}\parallel}}{D_{\pm}} K_L , \qquad \text{(B7)}$$

where $D_{\pm}$ is the common denominator term defined by Eq. (B5). For reasons discussed below, the terms dependent on spin-transfer from the deuteron tensor polarization components were ignored. As before, the $\pm$ superscripts indicate the sign of the deuteron vector polarization, whereas the symbols $\mathbf{p}_{\mathbf{d}\parallel}$ and $\mathbf{p}_{\mathbf{d}\perp}$ represent the magnitudes of the components of the deuteron vector polarization in the reaction plane (S, or L depending on the configuration) or normal (N) to the reaction plane, respectively. For generality, a simplified spin-transfer coefficient (K) was introduced (with the factor of $\frac{3}{2}$ absorbed). Its single subscript represents the direction of the relevant proton spin component produced by the particular spin-transfer from the specific deuteron spin ($\parallel$ or $\perp$) involved. No transfer of spin occurs between the normal (N) deuteron polarization and the sideways or longitudinal proton polarization (or vice versa) because of parity conservation [20].

In principle, the contribution of spin-transfer from the deuteron tensor terms should be included. However, the values of the tensor spin-transfer coefficients are not known experimentally and are poorly defined by the existing PWA fits. Fortunately, neglect of these terms could be justified for the following reasons: first, their contribution is weighted by the typically small deuteron tensor polarizations (<0.10) [as given in Eqs. (B1) and (B2)]; and second, since the signs of the non-negligible tensor components [$\mathbf{p}_{LL}$ and $(\mathbf{p}_{SS} - \mathbf{p}_{NN})$] remain unchanged when the deuteron vector polarization is reversed [see Eqs. (B4)], such terms can be grouped with the systematic error terms $\mathcal{S}_{S/N}$ of Eq. (B6), and treated as described below.

The result of inserting relations (B7) into (B6) is

$$D^{+} P'^{+}_{N} = f_N (P_{\mathcal{N}} + R\mathbf{p}_{\mathbf{d}\perp} K_N) + g_N R\mathbf{p}_{\mathbf{d}\parallel} K_S + h_N R\mathbf{p}_{\mathbf{d}\parallel} K_L + \mathcal{S}_N ,$$

$$D^{-} P'^{-}_{N} = f_N (P_{\mathcal{N}} - \mathbf{p}_{\mathbf{d}\perp} K_N) - g_N \mathbf{p}_{\mathbf{d}\parallel} K_S - h_N \mathbf{p}_{\mathbf{d}\parallel} K_L + \mathcal{S}_N ,$$

$$D^{+} P'^{+}_{S} = f_S (P_{\mathcal{N}} + R\mathbf{p}_{\mathbf{d}\perp} K_N) + g_S R\mathbf{p}_{\mathbf{d}\parallel} K_S + h_S R\mathbf{p}_{\mathbf{d}\parallel} K_L + \mathcal{S}_S ,$$

$$D^{-} P'^{-}_{S} = f_S (P_{\mathcal{N}} - \mathbf{p}_{\mathbf{d}\perp} K_N) - g_S \mathbf{p}_{\mathbf{d}\parallel} K_S - h_S \mathbf{p}_{\mathbf{d}\parallel} K_L + \mathcal{S}_S . \qquad \text{(B8)}$$

For convenience, the magnitude of each deuteron polarization is expressed in terms of the magnitude of the negative polarization, $|\mathbf{p}^{-}_{\mathbf{d}}|$:

$$\mathbf{p}_{\mathbf{d}} = |\mathbf{p}^{-}_{\mathbf{d}}| \quad \text{and} \quad |\mathbf{p}^{+}_{\mathbf{d}}| = R|\mathbf{p}^{-}_{\mathbf{d}}| = R\mathbf{p}_{\mathbf{d}}$$

and the signs of the deuteron polarizations are indicated explicitly in Eq. (B8).

The terms involving the h_i coupling coefficients were disregarded since these coefficients were about two orders of magnitude smaller than the corresponding f_i and g_i coefficients (implying little coupling between the longitudinal polarization at the target and the transverse components at the polarimeter). Although this results in four equations involving the five unknown quantities $P_{\mathcal{N}}$, K_S, K_N, $\mathcal{S}_N$, and $\mathcal{S}_S$, extraction of the quantities of interest is straightforward.

By taking differences between the pairs of Eqs. (B8), $P_{\mathcal{N}}$ as well as $\mathcal{S}_N$ and $\mathcal{S}_S$ are eliminated, and thus

$$D^{+} P'^{+}_{N} - D^{-} P'^{-}_{N} = f_N (R+1)\mathbf{p}_{\mathbf{d}\perp} K_N + g_N (R+1)\mathbf{p}_{\mathbf{d}\parallel} K_S ,$$

$$D^{+} P'^{+}_{S} - D^{-} P'^{-}_{S} = f_S (R+1)\mathbf{p}_{\mathbf{d}\perp} K_N + g_S (R+1)\mathbf{p}_{\mathbf{d}\parallel} K_S . \qquad \text{(B9)}$$

From these, the pertinent parameters are readily obtained:

$$K_S\mathbf{p}_{\mathbf{d}\parallel}=\frac{(D^+P_S'^+-D^-P_S'^-)-(D^+P_N'^+-D^-P_N'^-)(f_S/f_N)}{g_S-g_N(f_S/f_N)}\frac{1}{(R+1)}, \tag{B10}$$

similarly,

$$K_N\mathbf{p}_{\mathbf{d}\perp}=\frac{(D^+P_N'^+-D^-P_N'^-)-(D^+P_S'^+-D^-P_S'^-)(g_N/g_S)}{f_N-f_S(g_N/g_S)}\frac{1}{(R+1)}. \tag{B11}$$

An important feature of Eqs. (B10) and (B11) is the absence of the systematic error terms $\mathcal{S}_{S/N}$ (which also include contributions from tensor spin transfer). Such a cancellation occurs for those systematic errors which are instrumental in nature and constant in time.

Finally, in order to extract the specific spin-transfer parameters it was necessary to determine, for each experimental configuration, the values of the deuteron polarization components appearing on the left-hand side of Eqs. (B11) and (B10). These components are defined by the angles β and γ of Eq. (B4).

In the case of the K_{LS} configuration, the target was polarized along an axis parallel to the incident pion beam, the L axis. Since the pion trajectory was parallel to the magnetic field of the target and thus undeflected by it, the deuteron spins had a pure longitudinal projection ($\beta=0°$) in the COMAF.

For the transversely polarized targets associated with the K_{SS} and K_{NN} configurations, however, the appropriate N and S axes were, in general, *not* parallel to the fixed direction of the deuteron polarization set by the target field direction. This complication had two sources: the bending of both the incident pion and emerging proton trajectories in the magnetic field; as well as the fact that the N and S axes, depending as they did on the direction of $\hat{k}_p^*$, varied due to the finite acceptance of the polarimeter. This had two consequences: a reduction in the projection of the deuteron polarization along the axis of interest; and the possible introduction of an orthogonal deuteron polarization component which could result in other spin-transfer contributions. Since the bending of the pion trajectory by the magnetic field occurred in a plane which was orthogonal to the polarization vector, the value of β was fixed ($\beta=90°$) and the effects described here were simply characterized by the angle γ in Eq. (B4).

The value of γ was determined by projecting the fixed target polarization onto appropriate axes for each of many possible trajectory bins, spanning the acceptance of the polarimeter. An average projection, $\langle\cos\gamma\rangle$ and $\langle\sin\gamma\rangle$, onto each of the transverse axes was then obtained by weighting the projection associated with each trajectory bin by the relative number of events for that bin (as obtained from the data). In the case of the K_{NN} configuration, the result was a slight reduction of the normal polarization by a factor ($\langle\cos\gamma\rangle\sim0.99$). No orthogonal component was introduced since the net deuteron polarization projected onto the sideways axis of the COMAF cancelled when averaging over the polarimeter acceptance. For the K_{SS} configuration, however, the acceptance was such that there was a substantial net projection onto the normal axis ($\langle\cos\gamma\rangle\sim0.15$). Thus, in addition to a slightly reduced magnitude of the sideways polarization ($\langle\sin\gamma\rangle\sim0.98$), a small normal-to-normal spin-transfer component was introduced in the COMAF. In the analysis, however, this term was not considered since $\langle\cos\gamma\rangle$ was small and K_{NN} was expected to be near zero in the angular region applicable to the K_{SS} configuration ($\sim90°$ c.m.).

On this basis, Eqs. (B10) and (B11) could be readily adapted to the specific quantities of interest. Using Eqs. (B1), (B2), and (B7), and with the following substitutions into Eqs. (B10) and (B11): for K_{LS}: $\mathbf{p}_{\mathbf{d}\parallel}\Rightarrow\mathbf{p}_{\mathbf{d}}$ and $K_S\Rightarrow\frac{3}{2}K_{LS}$, for K_{SS}: $\mathbf{p}_{\mathbf{d}\parallel}\Rightarrow\mathbf{p}_{\mathbf{d}}\langle\sin\gamma\rangle$ and $K_S\Rightarrow\frac{3}{2}K_{SS}$, for K_{NN}: $\mathbf{p}_{\mathbf{d}\perp}\Rightarrow\mathbf{p}_{\mathbf{d}}\langle\cos\gamma\rangle$ and $K_N\Rightarrow\frac{3}{2}K_{NN}$ we obtain for the K_{LS} configuration

$$K_{LS}=\frac{2}{3}\frac{1}{\mathbf{p}_{\mathbf{d}}}\frac{(D^+P_S'^+-D^-P_S'^-)-(D^+P_N'^+-D^-P_N'^-)(f_S/f_N)}{g_S-g_N(f_S/f_N)}\frac{1}{(R+1)}, \tag{B12}$$

for the K_{SS} configuration

$$K_{SS}=\frac{2}{3}\frac{1}{\mathbf{p}_{\mathbf{d}}\langle\sin\gamma\rangle}\frac{(D^+P_S'^+-D^-P_S'^-)-(D^+P_N'^+-D^-P_N'^-)(f_S/f_N)}{g_S-g_N(f_S/f_N)}\frac{1}{(R+1)}, \tag{B13}$$

and for the K_{NN} configuration

$$K_{NN}=\frac{2}{3}\frac{1}{\mathbf{p}_{\mathbf{d}}\langle\cos\gamma\rangle}\frac{(D^+P_N'^+-D^-P_N'^-)-(D^+P_S'^+-D^-P_S'^-)(g_N/g_S)}{f_N-f_S(g_N/g_S)}\frac{1}{(R+1)}. \tag{B14}$$

The quantity $P_{\mathcal{N}}$ can also be extracted from the experimental data. Addition of the pairs of Eqs. (B8) (ignoring terms involving h_i) yields

$$D^+P'^+_N + D^-P'^-_N = f_N[2P_{\mathcal{N}} + (R-1)\mathbf{p}_{\mathbf{d}\perp}K_N] + g_N(R-1)\mathbf{p}_{\mathbf{d}\parallel}K_S + 2\mathcal{S}_N,$$
$$D^+P'^+_S + D^-P'^-_S = f_S[2P_{\mathcal{N}} + (R-1)\mathbf{p}_{\mathbf{d}\perp}K_N] + g_S(R-1)\mathbf{p}_{\mathbf{d}\parallel}K_S + 2\mathcal{S}_S.$$

$P_{\mathcal{N}}$ is thus given by

$$P_{\mathcal{N}} = \frac{(D^+P'^+_N + D^-P'^-_N) - (D^+P'^+_S + D^-P'^-_S)(g_N/g_S) - \frac{3}{2}(R-1)\mathbf{p}_{\mathbf{d}\perp}K_{NN}[f_N - f_S(g_N/g_S)] - 2\mathcal{S}_N + 2(g_N/g_S)\mathcal{S}_S}{2[f_N - f_S(g_N/g_S)]}, \tag{B15}$$

where K_{NN} is obtained from Eq. (B14). Unlike the situation for Eqs. (B10) and (B11) the expression for $P_{\mathcal{N}}$ does contain the systematic error terms, $\mathcal{S}_N$ and $\mathcal{S}_S$. However, since the value of $P_{\mathcal{N}}$ is already accurately known from existing analyzing power data (A_{N0}), comparison of values extracted from our experiment, using Eq. (B15), with the known analyzing power data provides useful information concerning the possible existence of systematic errors in our experimental arrangement.

[1] H. Garcilazo and T. Mitzutani, *πNN Systems* (World Scientific, Singapore, 1990).
[2] T. Ericson and W. Weise, *Pions and Nuclei* (Oxford University Press, Oxford, England, 1988).
[3] F. Foroughi, J. Phys. G **8**, 1345 (1982).
[4] B. Blankleider and I. R. Afnan, Phys. Rev. C **31**, 1380 (1985)
[5] D. V. Bugg, A. Hasan, and R. L. Shypit, Nucl. Phys. **A477**, 546 (1988).
[6] I. I. Strakovskii, A. V. Kravtsov, and M. G. Ryskin, Yad. Fiz. **40**, 429 (1984).
[7] N. Hiroshige, W. Watari, and M. Yonezawa, Prog. Theor. Phys. **72**, 1146 (1984).
[8] D. V. Bugg, Nucl. Phys. **A437**, 534 (1985).
[9] G. Cantale *et al.*, Helv. Phys. Acta **60**, 398 (1987).
[10] D. A. Hutcheon *et al.*, Nucl. Phys. **A503**, 649 (1989).
[11] R. Abegg *et al.*, Nucl. Phys. **A539**, 573 (1992).
[12] S. E. Turpin *et al.*, in *The Proceedings of the Tenth International Conference on Few-Body Problems in Physics*, edited by B. Zeitnitz (Elsevier, New York, 1984), Vol. 2, p. 189.
[13] B. Bonin *et al.*, Nucl. Instrum. Methods Phys. Res. A **288**, 389 (1990).
[14] P. Herczeg, in *Symmetries and Fundamental Interactions in Nuclei*, edited by W. C. Haxton and E. M. Henley (World Scientific, Singapore, 1995), p. 89.
[15] R. G. Sachs, *The Physics of Time Reversal* (The University of Chicago Press, Chicago, 1987).
[16] G. Waters *et al.*, Nucl. Instrum. Methods **153**, 401 (1978).
[17] D. Besset, Q. H. Do, B. Favier, L. G. Greeniaus, R. Hess, C. Lechanoine, D. Rapin, D. W. Werren, and C. Weddigen, Nucl. Instrum. Methods **166**, 379 (1979).
[18] R. D. Ransome, S. J. Greene, C. L. Hollas, B. E. Bonner, M. W. McNaughton, C. L. Morris, and H. A. Thiessen, Nucl. Instrum. Methods **201**, 309 (1982).
[19] G. D. Wait *et al.*, in *The 8th International Symposium on High Energy Spin Physics*, edited by K. Heller, AIP Conf. Proc. No. 187, (AIP, New York, 1988), p. 1260.
[20] M. Simonius, in *Theory of Polarization Measurements, Observables, Amplitudes and Symmetries*, edited by D. Fick, Lecture Notes in Physics Vol. 30, (Springer-Verlag, Berlin, 1974), p. 38.
[21] Madison Convention, in *Polarization Phenomena in Nuclear Reactions*, edited by H. H. Barschall and W. Haeberli (University of Wisconsin Press, Madison, WI, 1971).
[22] A. Feltham *et al.*, Phys. Rev. Lett. **66**, 2573 (1991).
[23] TRIUMF Users Handbook, 1987, second ed. (unpublished).
[24] C. L. Morris, H. A. Theissen, and G. W. Hoffman, IEEE Trans. Nucl. Sci. **NS-25(1)**, 141 (1978).
[25] R. Henderson, O. Hausser, K. Hicks, C. Gunther, W. Faszer, R. Sawafta, and N. Poppe, Nucl. Instrum. Methods Phys. Res. A **254**, 61 (1987).
[26] A. H. Walenta, Nucl. Instrum. Methods **151**, 461 (1978).
[27] L. G. Atencio, J. F. Amann, R. L. Boudrie, and C. L. Morris, Nucl. Instrum. Methods **187**, 381 (1981).
[28] A. Feltham, Ph.D. thesis, University of British Columbia, 1992.
[29] M. M. Pavan, Master's thesis, University of British Columbia, 1990.
[30] R. Henderson *et al.*, IEEE Trans. Nucl. Sci. **34**, 528 (1987).
[31] R. Henderson *et al.*, IEEE Trans. Nucl. Sci. **35**, 477 (1988).
[32] G. D. Wait and D. C. Healey, E331 internal report, TRIUMF (unpublished).
[33] G. D. Wait, J. V. Cresswell, P. P. J. Delheij, M. Hayden, D. C. Healey, and G. Waters, Helv. Phys. Acta **59**, 788 (1986).
[34] G. R. Smith *et al.*, Nucl. Instrum. Methods Phys. Res. A **254**, 263 (1987).
[35] D. Besset *et al.*, Nucl. Instrum. Methods **184**, 365 (1981).
[36] D. Besset, B. Favier, L. G. Greeniaus, R. Hess, C. Lechanoine, D. Rapin, and D. W. Werren, Nucl. Instrum. Methods **166**, 515 (1979).
[37] M. W. McNaughton *et al.*, Nucl. Instrum. Methods Phys. Res. A **241**, 435 (1985).
[38] S. MayTal-Beck *et al.*, Phys. Rev. Lett. **68**, 3012 (1992).
[39] J. Aclander *et al.*, Phys. Lett. B **300**, 19 (1993).
[40] A. Saha, K. K. Seth, D. Kielczewska, S. Iversen, M. Kaletka, D. Barlow, and D. Smith, Phys. Rev. Lett. **51**, 759 (1983).
[41] P. Walden (private communication).
[42] R. A. Abegg *et al.*, Nucl. Instrum. Methods Phys. Res. A **306**, 432 (1991).
[43] E. Aprile-Giboni, R. Hausammann, E. Heer, R. Hess, C. Lechanoine-Leluc, W. Leo, S. Morenzoni, Y. Onel, and D. Rapin, Nucl. Instrum. Methods **215**, 147 (1983).

[44] R. A. Arndt, I. I. Strakovsky, R. L. Workman, and D. V. Bugg, Phys. Rev. C **48**, 1926 (1994).
[45] B. Blankleider (private communication).
[46] J. Niskanen (private communication).
[47] B. Blankleider and A. N. Kvinikhidze, Few-Body Syst. Suppl. **7**, 294 (1994).
[48] J. A. Niskanen Phys. Rev. C **49**, 1285 (1994).
[49] A. Matsuyama and T.-S. H. Lee, Nucl. Phys. **A526**, 547 (1991).
[50] U. Schryber *et al.*, in *Proceedings of the 14th International Conference on Cyclotrons and their Applications*, Cape Town, South Africa, 1995, edited by J. C. Cornell (World Scientific, Singapore, 1996).
[51] W. Meyer, in *The 11th International Symposium on High Energy Spin Physics*, edited by K. Heller and S. Smith, AIP Conf. Proc. No. 343 (AIP, New York, 1995), p. 495.
[52] G. Gammel, P. Keaton Jr., and G. Ohlsen, *Polarization Phenomenon in Nuclear Reactions* (University of Wisconsin Press, Madison, WI, 1971), p. 411.
[53] G. R. Smith *et al.*, Phys. Rev. C **30**, 980 (1984).
[54] V. Bargmann, L. Michel, and V. L. Telegdi, Phys. Rev. Lett. **2**, 435 (1959).